

## Rainbows in nature: recent advances in observation and theory

This content has been downloaded from IOPscience. Please scroll down to see the full text.

2016 Eur. J. Phys. 37 063001

(<http://iopscience.iop.org/0143-0807/37/6/063001>)

View [the table of contents for this issue](#), or go to the [journal homepage](#) for more

### Download details:

IP Address: 77.200.184.34

This content was downloaded on 16/11/2016 at 10:00

Please note that [terms and conditions apply](#).

You may also be interested in:

[Comparison of the 'glory' with coherent backscattering of light in turbid media](#)

Ralf Lenke, Ulrich Mack and Georg Maret

[Optics demonstrations using cylindrical lenses](#)

Dragia Ivanov and Stefan Nikolov

[3D transport of solar radiation in clouds](#)

Anthony B Davis and Alexander Marshak

[Laser diffraction microscopy](#)

P Schall

[On the colours of spider orb-webs](#)

Wilfried Suhr and H Joachim Schlichting

[Single metal nanoparticles](#)

P Zijlstra and M Orrit

## Review

# Rainbows in nature: recent advances in observation and theory

**Alexander Haußmann**

Pfotenhauerstr. 32/701, D-01307 Dresden, Germany

E-mail: [alexander.haussmann@tu-dresden.de](mailto:alexander.haussmann@tu-dresden.de)

Received 12 February 2016

Accepted for publication 1 July 2016

Published 26 August 2016



CrossMark

## Abstract

This topical review presents an overview of the common and less common observations of rainbows in natural rainfall, and the theoretical concepts that have been developed for their explanation. Mainly throughout the last 20 years, many new and intriguing effects have been photographed or documented for the first time, such as higher-order (tertiary, quaternary, etc) and twinned rainbows, as well as rainbows generated by nearby artificial light sources. In order to provide a sound explanation, the inclusion of natural non-spherical (i.e. oblate) raindrop shapes as well as natural broad polydisperse raindrop distributions into the classical rainbow theory (Lorenz–Mie and Debye scattering) is outlined. Thus, the article provides a condensed up-to-date synopsis complementing classical textbooks and earlier reviews on the physics of rainbows. It is intended to serve both active sky observers as well as physics teachers who want to keep up with current developments in the field.

Keywords: higher-order rainbows, twinned rainbows, divergent-light rainbows

(Some figures may appear in colour only in the online journal)

## 1. Introduction

Not many people can escape the fascination evoked by one of nature's most magnificent play of colors: a bright, double rainbow spanning wide across the sky, promising the withdrawal of a recent rain shower and the return of the Sun. We share this fascination along with our ancestors; mankind has always been stunned by rainbows, inspiring many religious interpretations such as God's covenant with Noah in the Genesis flood narrative or Bifröst, the bridge to Asgard, in Norse mythology. In later times, rainbows became a subject for both scientists and artists alike. This review will focus exclusively on the scientific part—which is in itself already overwhelmingly extensive. Seemingly all important philosophers and

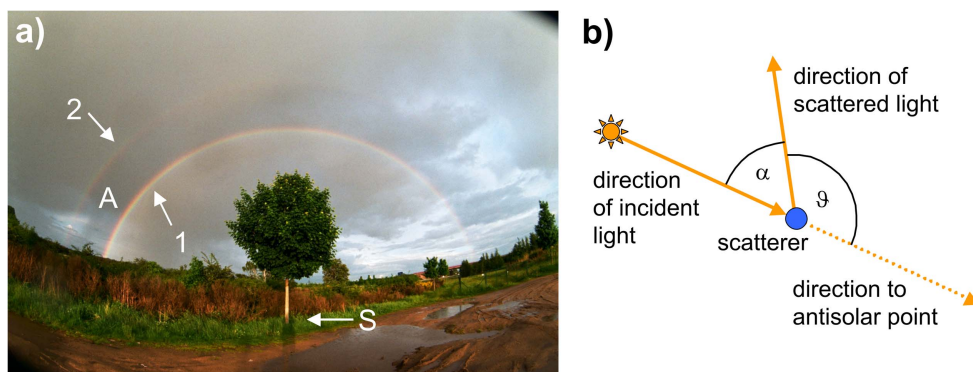


**Figure 1.** (a) Typical well-developed double rainbow display, including the primary rainbow (1), secondary rainbow (2), the shadow of the observer's head (S) and Alexander's dark band (A). (b) Sketch of the scattering geometry, defining the scattering angle  $\vartheta$  and the angle towards the antisolar point  $\alpha$ .

physicists throughout the past centuries who were concerned with questions about light and optics have contributed to the rainbow's scientific history. As of now, a substantial number of reviews and books from the 20th and 21st centuries have compiled the classical knowledge about the rainbow phenomenon [1–8], so one might ask: why is there the need for yet another review?

One reason is that over the past 20 years, the amount of reports of unusual rainbows, supported by reliable photographs, has drastically increased. Furthermore, centuries-old debates about the existence (or better 'detectability') of natural higher-order rainbows beyond the well-known primary and secondary have finally been settled—and indeed in a positive way. These advances are mostly due to a rising number of amateur observers equipped with ever improving digital cameras and close cooperation in national networks, e.g. the German 'Arbeitskreis Meteore (AKM) e.V.' [9]. On the international level, the 'Light and Color in Nature' conference series has proven to be a reliable platform to establish links between practical observers and scientists with a more theoretical approach towards optics. Moreover, several ideas on how to employ rainbow scattering for sensor applications have been inspired by natural observations and methods of their analysis. All this keeps the field of rainbow research scientifically vivid and active.

Against this background it is regrettable that the rainbow, like other atmospheric effects, is often covered only very briefly at all education levels from primary school to university. It is thus a further goal of this review to promote rainbows as apt examples not only for reflection and refraction on and in water spheres, but also for more advanced optical effects such as interference and multiple scattering. No expensive equipment is needed for these observations—an ordinary camera, and optionally a polarizer, are fully sufficient. However, natural rainbows do not occur too frequently (typically 10–20 days per year in Germany, or 40–70 days in the English Midlands [10]), but luckily it is possible to study rainbow scattering using artificial drop sources without great expense.

The review is structured as follows: section 2 contains the classic history of rainbow theories up to Lorenz–Mie and Debye scattering. Section 3 extends the theoretical considerations towards natural non-spherical drop shapes and broad drop-size distributions. Sections 4–7 are each devoted to a rainbow effect which gained attention throughout recent years: special locations, twinned bows, higher-order bows, and divergent-light bows.

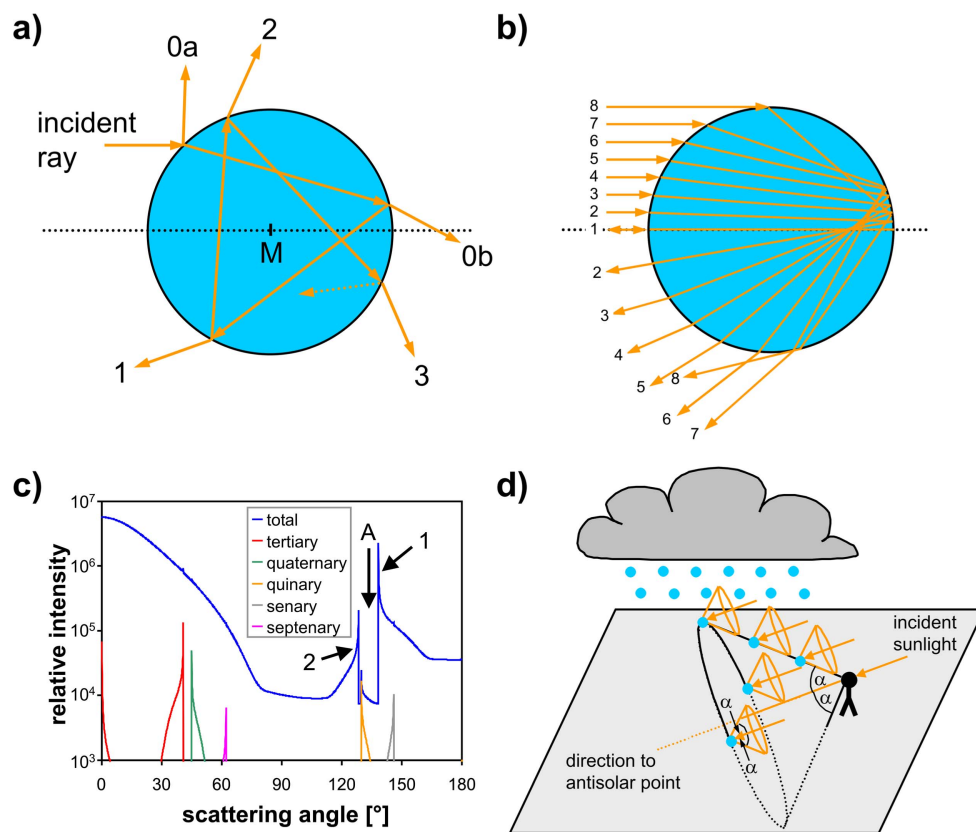


**Figure 2.** (a) Classification of ray paths through a water drop, indicating the rainbow orders to which the exiting rays contribute (for rays of classes 1 and higher). 0a and 0b rays do not produce rainbows. (b) Raytracing calculation for the primary rainbow, with path 7 depicting the Descartes ray of extremal deflection (adapted from [7]). Due to the spherical symmetry, it is sufficient to treat only a planar section through the drop's center. (c) Scattering intensity distribution of a single water drop according to geometric optics, relative refractive index (air/water)  $n = 1.3355$ , point like light source (calculated with MiePlot [12]), 1: primary rainbow, 2: secondary rainbow, A: Alexander's dark band. The contributions of the higher-order rainbow paths are depicted separately. (d) Geometric relation between the light emitted by an individual drop and the perception of the observer for the primary bow (adapted from [4]). Only a few sunlit drops under the cloud are depicted here, which are, moreover, located at the right positions to successfully send their scattered light to the observer. The colors of the rainbow are omitted for the sake of a clearer presentation. An analogous picture could be drawn for the secondary rainbow.

Section 8 summarizes useful hints for those who want to chase rare rainbows themselves. Conclusions and an outlook are given in section 9.

## 2. Evolution of traditional rainbow theories

Classical rainbows are colored segments of circles that appear in the celestial region opposite the Sun when sunlit raindrops are present in this viewing direction. More precisely, the so-

called primary rainbow appears at angle of about  $42^\circ$  from the antisolar point, which is marked approximately by the shadow of the observer's head. Red is located at the outside rim, and the sky is considerably brighter inside the rainbow than outside. The opposite holds for the secondary rainbow: red lies inside, and the sky appears brighter to the outside. Its angular radius is larger (about  $51^\circ$ ) and all its features usually appear fainter than those of the primary. The red rims of both rainbows face each other, and the dark space in between them is known as Alexander's dark band (after Alexander of Aphrodisias,  $\sim 200$  AD) (see figure 1(a)). Rainbows are intangible, in the sense that they are nothing more than scattered sunlight reaching the observer from certain directions, or, alternatively expressed, they are heavily distorted images of the Sun itself. Furthermore, their light is strongly polarized in the tangential (or azimuthal) direction, with an intensity ratio between the azimuthal and radial component of 25:1 for the primary and 9.4:1 for the secondary [11].

Why and how rainbows form are questions that arose at the very beginning of natural philosophy. Aristotle postulated that rainbows result from sunlight reflected from distant clouds, though 'artificial rainbows' in the spray generated by oars were already known to the Greeks. It took several centuries to develop and prove the idea that individual scattering from (nearly) spherical water drops is responsible for the rainbow formation. The Arab scientist Avicenna (980–1037) was aware of the necessity of sunlit water drops, the Dominican scholar Theodoric of Freiberg (about 1250–1310) could demonstrate the similarity of the scattering light pattern emerging from a water-filled glass sphere and the rainbow, and finally Descartes published his now famous rainbow theory as a chapter in his *Discours de la méthode* in 1637. In that he describes similar experiments as done by Theodoric, but also performs quantitative ray tracing for parallel sunlight using the correct law of refraction. This analysis correctly predicted high concentrations of rays emerging from the spherical drop at the rainbow scattering angles (see figure 1(b)) of  $\vartheta \approx 138^\circ$  (corresponding to  $\alpha \approx 42^\circ$ ) and  $\vartheta \approx 129^\circ$  (corresponding to  $\alpha \approx 51^\circ$ ) for one and two internal reflections, respectively (figure 2(a)). These are due to extrema in the deflection function (scattering angle versus impact parameter) [7], and still today these extremal scattering angles and the ray paths that generate them are named after Descartes. No ray can be deflected less than  $\approx 138^\circ$  along a ray path involving exactly one internal reflection (figure 2(b)), and no ray can be deflected more than  $\approx 129^\circ$  along a ray path involving exactly two internal reflections: thus it is obvious why the region between the two rainbows appears dark.

We would, however, not expect complete darkness in Alexander's dark band. This is not only due to an 'extrinsic' background from skylight, clouds, or diffuse multiple scattering from other raindrops as common in natural rainbow displays, but light also enters this region from other ray paths than the two previously discussed. As seen from figure 2(a), there are, additionally, externally reflected rays (0a), transmitted rays (0b), and paths with  $>2$  internal reflections. The latter give rise to so-called higher-order rainbows (see section 6), and although their number is in principle infinite, only the first few of them provide contributions to the total scattering intensity which are strong enough to be detected with current digital cameras in natural rainbow displays. This total intensity according to Descartes' theory, refined by taking into account Fresnel's formulas for the reflected and transmitted light intensities, is depicted in figure 2(c), including rainbows up to the seventh order (see section 6 for the motivation for going up to this specific number). The rays of classes 0a and 0b do not exhibit an extremal value in their deflection function, thus they do not produce any rainbows. Nonetheless 0a rays add to the diffuse 'intrinsic' background in Alexander's dark band and elsewhere. Most noticeable is the intense forward scattering stemming from the 0b rays, which consequently bears the name 'zero order glow'.

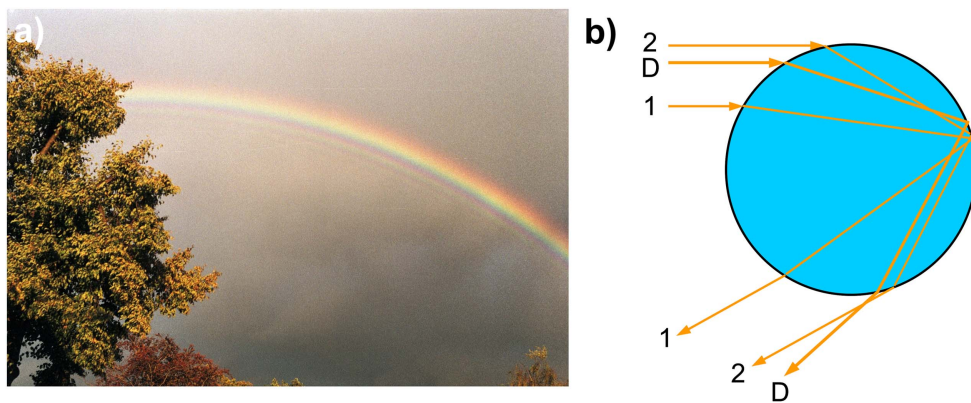


**Figure 3.** (a) Pronounced sequence of supernumerary arcs inside the primary rainbow. (b) Sketch of two rays 1 and 2 with the same scattering angle, leading to interference (D = Descartes ray) (adapted from [7]).

At this point, it has to be noted that such single-drop calculations and experiments as performed by Descartes (or today's researchers) describe in the first instance not a natural rainbow, but the scattering light distribution emerging from that individual drop only. This theory predicts that the drop will emit, amongst others, luminous cones with opening angles of  $\alpha \approx 42^\circ$  and  $\alpha \approx 51^\circ$ , corresponding to the primary and secondary rainbow ray path. Under natural conditions, myriads of sunlit drops emit such cones, with only a small portion of them being located at the right positions to send light into the observer's eye, i.e. contributing to the actual phenomenon called 'the rainbow', which shall be understood as the sensory perception of a single observer. These contributing drops have to be located themselves on  $42^\circ$  and  $51^\circ$  cones, which are, however, now centered at the observer's eye, and point towards the antisolar direction (see figure 2(d)). This implies that two nearby observers (or even the two eyes of the same person) do not see exactly the 'same' rainbows, in the sense that they see light emitted from different drops. Some years ago, there was even a rather elaborate philosophical discussion in the German observer's network on the question whether rainbows, strictly interpreted, may exist at all when no observing eye is present, as in this case the necessary selector for the numerous scattering cones of all sunlit raindrops is missing [13].

The previous argumentation is a special case of a more general principle, known under the name 'sky transform' [14]. It is straightforward to show that an observer embedded in the center of a spherical, uniform, and dilute assembly of identically constituted, shaped and oriented scatterers<sup>1</sup> illuminated with parallel light will record basically the same scattering light pattern as projected onto the inner wall of a collection sphere by a single representative of these scatterers placed in the middle of the sphere and illuminated from the same direction. The only differences are that the absolute intensities will not be equal (which does not matter here, as only relative intensities are of interest), and both patterns are spatially inverted with respect to each other. This inversion does not, however, influence the highly symmetric circular rainbows from spherical drops. It will, however, matter for non-spherical drops (section 3.1). The assumed low density of scatterers ensures that multi-scattering effects are negligible, i.e. the incident light is only unnoticeably extinguished throughout the scatterers'

<sup>1</sup> The volume of the assembly of illuminated scatterers has to be finite in the single scattering limit, otherwise the intensity reaching the observer would diverge. The spherical shape ensures that the contributing path of scatterers has an equal length for each viewing direction. For the realistic situation, see section 3.2.

**Table 1.** Descartes angles for the first seven rainbow orders for three selected wavelengths, corresponding roughly to the RGB sensitivity maxima of a common SLR camera sensor. The values are given as scattering angles (angular distance from the Sun) for a water and air temperature of 15 °C (resulting in the noted values for the relative refractive index  $n$ ). Orders 1, 2, and 5 appear in the backward hemisphere (i.e. towards the antisolar point), orders 3 and 4 appear in the forward hemisphere (i.e. towards the Sun). The last column contains the angular spread between red and blue. In reality, the angular diameter of the Sun ( $\sim 0.5^\circ$ ) and a further spread due to wave-optics effects (especially for small drops) have to be taken into account to describe correctly the rainbows' width.

Rainbow order	Red ( $\lambda = 620$ nm, $n = 1.3324$ )	Green ( $\lambda = 530$ nm, $n = 1.3355$ )	Blue ( $\lambda = 460$ nm, $n = 1.3390$ )	Angular spread  blue-red
1	137.8°	138.3°	138.8°	0.9°
2	129.3°	128.5°	127.6°	1.7°
3	41.9°	40.8°	39.6°	2.4°
4	43.4°	44.9°	46.5°	3.1°
5	127.9°	129.6°	131.6°	3.7°
6	148.1°	146.1°	143.8°	4.4°
7	64.5°	62.2°	59.5°	5.0°

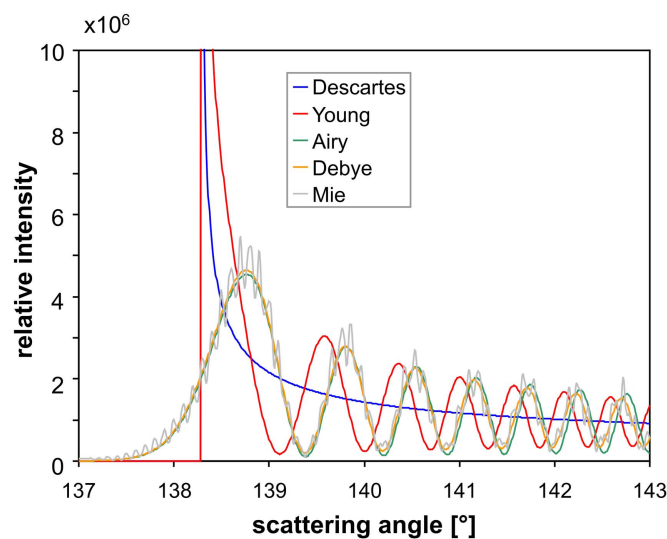


**Figure 4.** Prediction of the intensity distribution of the primary rainbow according to various optical theories (calculated with MiePlot [12] for a point-like sun, relative refractive index  $n = 1.3355$ ,  $\lambda = 530$  nm, and drop radius  $a_0 = 0.1$  mm). With the exception of Mie theory, only the contributions to the primary rainbow are shown.

assembly (=low optical thickness), and the single-scattered light from more remote drops reaches the observer unhindered.

Up to this point in the scientific history the rainbow, no satisfactory physical explanation for its colors was provided. It was Newton who showed that white sunlight is the superposition of many spectral colors, and that the index of refraction of a medium such as water

depends on the color. Therefore the values of the Descartes angles are slightly different for each color, and this angular dispersion increases with the rainbow order (see table 1). Henceforth, the primary rainbow has become the prototype of a ‘spectrum’ as realized in nature, though it differs considerably from Newton’s laboratory prism spectra, e.g. by the presence of supernumerary arcs (see below). Even today, any accidental spectra formed by refraction through sunlit ground glass panes or diffraction from CDs are incorrectly referred to by many people as ‘rainbows’. As Newton was (mostly) an advocate of the corpuscular theory of light, it was the merit of Young to link color with wavelength and to provide the first explanation of the spurious ‘supernumerary arcs’ that are occasionally visible inside the primary rainbow (see figure 3(a)) and very rarely outside the secondary [15]. Slightly apart from the Descartes angle inside the primary and outside the secondary, two ray paths exist for the same scattering direction (see figure 3(b)). Their difference in optical path length leads to either constructive or destructive interference, resulting in an characteristic intensity oscillation with respect to the scattering angle (and, of course, the wavelength). As the path length differences depend on the drop radius, the size of drops now becomes an important parameter in the theory—in Descartes’ view, all drops produce the same rainbows regardless of their size, as long as their shape matches an exact sphere. Young’s theory correctly predicts a denser sequence of supernumeraries as the drop size increases.

Young’s theory was, however, not complete, as diffraction at the Descartes angle (also named ‘caustic’, as rainbows can be understood as ‘burning curves’) as well as  $90^\circ$  phase shifts related to the crossing of focal lines were not accounted for [16]. Thus, the steeply declining intensity pole at the Descartes angle remains, and, moreover, the absolute positions of the supernumerary maxima are not predicted at the proper scattering angles (see figure 4). These difficulties troubled rainbow theorists until recently, when Young’s method, refined with Fresnel’s formulas, was revived to describe the scattering from non-spherical raindrops (see section 3.1) [17]. Fresnel’s formulas furthermore allow an elegant explanation of the strong polarization of the rainbow, which was first observed by Biot in 1811 [18]. The internal reflection angle for the Descartes ray of the primary falls very close to Brewster’s angle, at which no p-polarized light (corresponding to the radial direction as seen from the observer) is reflected. The angle of the two internal reflections for the secondary’s Descartes ray is a bit further off from the Brewster value, therefore its polarization is less strong.

To account for the diffraction effects in the neighborhood of the Descartes angle, Airy went beyond the ray approximation and employed true wave optics [1, 7, 19]. The emitted wave front exhibits a rather complex, cusped shape far from the drop, but when tracing it back it turns out that the important part can be very well approximated by a simple cubic parabola. The application of Huygen’s principle leads then to the famous ‘rainbow integral’. The solution for a monochromatic light wave amplitude is given by a special kind of mathematical function, which was later named after Airy [7]. The (relative) intensity is then easily calculated by squaring this amplitude. To obtain a realistic description of the rainbow, this calculation has to be carried out for multiple wavelengths of the solar spectrum, and the resulting multispectral data have to be mapped to the RGB color space. These very laborious steps were first taken by Pernter [1] for the primary bow, relying on one of the first color space model based on Maxwell’s tristimulus theory.

Again, Airy’s theory was not the final answer to the rainbow problem, as the shape of the wavefront is rendered only approximately and, moreover, the amplitude is assumed to be constant along the wavefront. The most severe consequences of this are that the Airy approximation is only valid in the immediate neighborhood (i.e. some degrees) of the respective Descartes angle, and only the strong, azimuthally polarized component is represented satisfactorily well for drops that are not too small (radius  $>\approx 0.05$  mm [7]). Several

efforts have been made to overcome these limitations, culminating in the extensive calculations of Möbius [20]. Much later it was shown by Können that at least the polarization issue—a consequence of the drastically varying Fresnel coefficient for the radial component at the internal reflection—can be corrected, while retaining the analytical elegance of the original Airy theory [21]. Furthermore, the Airy theory can be generalized to describe higher-order rainbows as well, though the minimal drop size threshold which guarantees the validity of the theory's assumptions increases with the rainbow order [22].

By the end of the 19th century, the time was ripe again for yet another new theoretical concept—the analytical description of scattering of a monochromatic plane wave from a dielectric sphere according to Maxwell's electrodynamics. This problem was solved by Lorenz in 1890 [23]. However, his contributions remained largely unregarded and most of the fame went to Mie, who published his own, equivalent solution in 1908 [24] (for some historical details, see also [25]). The main idea is the decomposition of the incident plane wave into a series of partial waves fitting to the spherical symmetry of the scatterer, the calculation of the scattering amplitude for each partial wave and the final recombination of these amplitudes. Theoretically, the partial wave series must be infinite to exactly match the incident plane wave; however, the output contributions drop quickly to zero from a certain summation index on. This crucial index limit depends on the ratio of the sphere's radius and the wavelength, and reaches values of about 1000–15 000 for typical raindrops. This was clearly out of range for manual calculations, thus the first Lorenz–Mie solutions for the rainbow problem could be obtained only after electronic computers became available by the second half of the 20th century.

Seemingly, the ultimate goal was then reached—the scattered light from a spherical drop, including the reflection at the surface, the direct transmission and the infinite series of rainbow orders (though only two are seen under normal circumstances) could be calculated with a high degree of precision [25]. But, the results were 'oracular' in the sense as there was no further insight into the deeper systematics of the scattering process—one could only get the 'complete' answer. This also included disturbing high frequency intensity oscillations in the scattering angle, stemming from the interference between different rainbow orders and the directly transmitted or reflected light (see figure 4). These are, however, not observed under natural conditions, as the only observable interference effects are the supernumerary arcs of one and the same rainbow order. This is due to the limited temporal coherence of sunlight, the Sun's angular diameter of about  $0.5^\circ$ , and the naturally broad and continuous distribution of raindrop sizes (see section 3.2) [26].

However, shortly after Mie the problem of a meaningful structuring of the scattering process was solved by Debye [27] for cylinders, and later extended to spheres by van der Pol and Bremmer [28]. The idea is to use a further series expansion for each partial wave, with each term corresponding to a certain number of surface interactions such as reflection and transmission. These contributions can be identified with the ray classes presented in figure 2(a).

With this decomposition, the limited coherence can be taken into account by adding up the intensities instead of the (complex) amplitudes of various rainbow orders. Thus all the flexibility and insight which is characteristic for the ray models of Descartes and Young is restored on this much more accurate level of Maxwell's electrodynamics. Furthermore, the Debye series is a very powerful tool to study other scattering effects such as the corona and the glory which become prominent for small water drops with radii  $<0.05$  mm in the forward and backward direction. The primary rainbows stemming from these very small drops (usually referred to as 'fogbows' or 'cloudbows') appear broad and white with large angular spaces towards and in between the supernumeraries. Figure 4 presents a comparison of all the

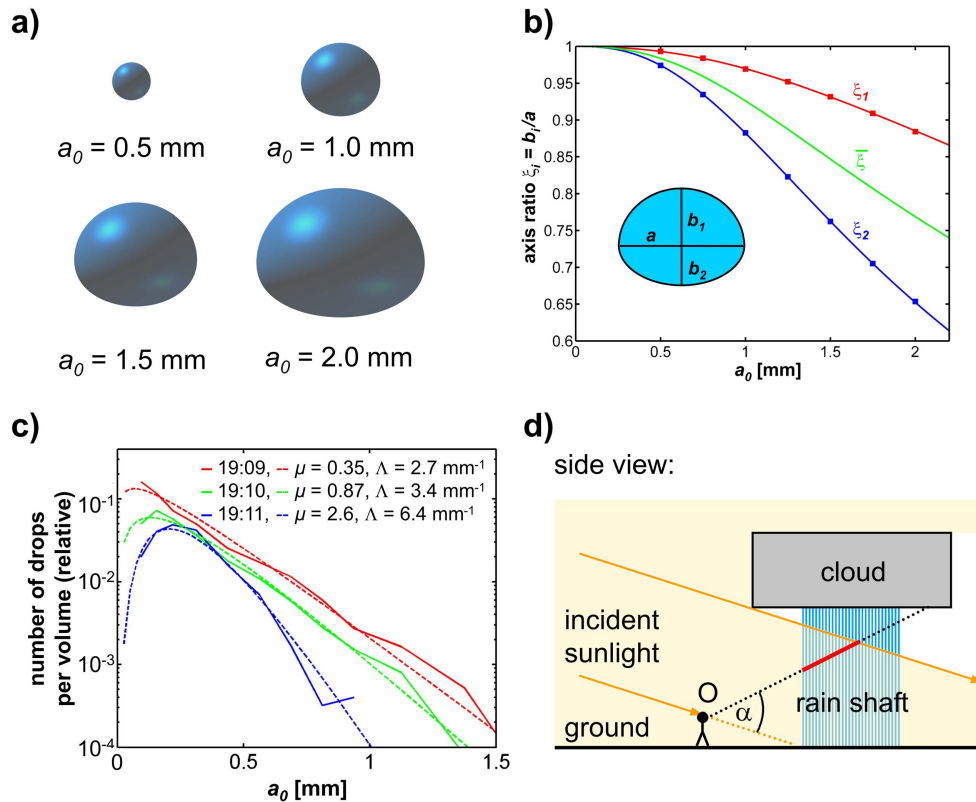


**Figure 5.** (a) Examples of raindrop shapes for various equivalent radii  $a_0$ , calculated with the model from [32]. Though drops for  $a_0 = 0.5$  mm still appear rather spherical here, their distortion is already high enough to result in considerably shifted rainbows. (b) Degrees of oblateness for the upper ( $\xi_1$ ) and lower ( $\xi_2$ ) half, as well as averaged over both halves ( $\bar{\xi}$ ) (reprinted from [38] with permission from OSA). (c) Temporal evolution of DSDs measured on 22 April 2012, near Göttingen, Germany, averaged over 1 min each (times are given in CEST), dashed: fits with formula (1) (fit parameters included in legend). (d) Sketch of the illumination geometry of a rain shower; the effective line of sunlit drops is marked red (adapted from [35]).

discussed theories for the vicinity of the primary rainbow for a drop radius of 0.1 mm and green light ( $\lambda = 530$  nm).

For completeness, it should be mentioned that the obstructively high number of terms in the partial wave series has inspired Nussenzveig in the 1970s to apply a modified Watson transform, leading to the so called complex-angular-momentum (CAM) theory of the rainbow [29]. However, nowadays the direct computation of the Lorenz–Mie or Debye series is feasible on ordinary desktop computers, e.g. with Laven’s MiePlot software [12], or self-written codes employing recursion algorithms for the evaluation of the involved Riccati–Bessel functions and Legendre polynomials [30]. The only critical issue is the numerical stability due to the high number of recursion steps.

### 3. Towards a realistic description: modern theoretical developments

#### 3.1. Realistic drop shapes

What mostly goes unnoticed in scientific discussions of the rainbow problem is that nature's rainbows are more than just a simple copy of the scattering pattern of a single, spherical water drop projected into the sky. First of all, raindrops are almost never truly spherical—the larger their size, the more oblate they become as a consequence of air drag as they fall down. The shape of falling raindrops has been calculated from basic principles [31, 32] and experimentally determined using video disdrometer techniques [33, 34]. Falling drops typically resemble an asymmetrically squashed sphere: the bottom part is flatter than the dome-like top, and the whole shape has sometimes been nicknamed a 'hamburger bun'. The size of such drops is characterized by the equivalent radius  $a_0$ , i.e. the radius of a sphere with the same volume as the drop. Figure 5(a) shows some typical examples for various equivalent radii, whereas figure 5(b) depicts the degrees of oblateness of two different half-spheroids being fitted to the upper and the lower half of the raindrop model from [32].

Clearly, the optical scattering properties will differ from what is known for spheres. This has already been noted by Venturi as early as 1814, who also performed calculations using an early and approximative drop model, with the aim of providing an explanation for the supernumerary arcs [36, 37]. However, precise raytracing calculations for the modern 'hamburger bun' model on the level of Descartes' and Young's theories become much more complicated compared to spheres, while the Lorenz–Mie and Debye approaches are not directly applicable at all [17, 38, 39]. In principle, a rigorous electrodynamic treatment could be accomplished using the T-matrix method for Chebyshev particles [40]. However, such calculations would require large numerical effort and bear the risk of stability problems, since the raindrops are relatively large compared to the wavelength. A common simplification of the problem is to treat a symmetric spheroidal drop instead, i.e. assuming the same degree of flattening for both the upper and lower part. Rainbows from such drops were discussed first by Möbius in 1907 [20]. Later work on this problem spanned a wide arc from ray optics [41–45] over Airy theory [46–49] towards a reformulation of the Debye series for elliptical geometry [50–52] and catastrophe theory [53, 54]. As it turns out, large drops with large amounts of oblateness lead to qualitatively new caustic features in primary, secondary (and tertiary, see section 6) rainbows.

Fortunately, most features of natural rainbows stem from relatively small drops ( $a_0 < \approx 1$  mm), for which the deviation from the spherical shape is not too large. Larger drops are very prone to oscillations [55] which are constantly re-instigated by eddy shedding at the drops' upper surface and/or collisions between the individual drops [56]. Therefore, no stable rainbows will result from them. Even in the absence of oscillations, the heavily distorted rainbows from such large drops will merge into a colorless background in a typical broad drop size distribution (see section 3.2). This is due to the fact the drop shape (and thus the rainbow position) is very sensitive to changes in the drop size in this radius regime, whereas smaller drops remain closer to the spherical shape within a larger size interval (see figure 5(b)). There is only one exception at the rainbows' bases for nearly horizontal sun light (see below). A final reason why large drops are less important is that their portion is already quite low in a typical drop size distribution, and even though they scatter more rainbow light per drop due to their larger cross section, the weighting of their overall contribution is not too high.

As the degree of distortion for the raindrops with  $a_0 < 1$  mm is still moderate, a perturbation theory treatment seems reasonable. This was already outlined in Möbius' original

work [20]: rainbows from slightly flattened drops will merely shift to a different position in the scattering angle without undergoing an inner change of the color and supernumerary pattern. Obviously, such a theory is not able to cover the emergence of new caustics when the distortion exceeds a certain amount. Originally Möbius treated only the top of the primary bow. The theory was later extended by Können to account for all positions along the circumference of both the primary and secondary [46]. Surprisingly, the secondary rainbow remains rather stable against moderate deformations, as long as they are symmetrical for the upper and lower part of the drop. This is due to an almost perfect compensation of the angular changes between the two internal reflections. The primary, on the other hand, strongly reacts to distortion, especially around its top.

The Möbius shift vanishes at both rainbows' bases for a zero solar elevation. In this case, the ray path is confined to a horizontal cross section through the drop. This cross section is circular for all drop sizes, thus the rainbows' position is in this case not influenced by a variable degree of oblateness in the vertical. This is one of the reasons why the rainbow bases usually appear brighter than the top, at which the contributions from different drop sizes are fanned out, especially for the larger drops [6, 57] (for other influences, see section 3.2). On the other hand, the combined effects of the Möbius shift and the drop size dependent evolution of width and supernumerary spacing for the primary rainbow result in a surprising consequence: visible supernumerary arcs at the primary's top are almost exclusively caused by drops with an effective radius in the range of 0.2–0.3 mm, and thus their angular spacing is very often the same [6, 41].

All these results were derived from the spheroidal approximation of raindrop shapes so far. The necessity to go beyond that for a more realistic description was pointed out as early as 1960 [58]. As of now, raytracing calculations for realistic equilibrium drop shapes, i.e. still neglecting oscillations [55], and deviations of the drops' symmetry axes from a strictly vertical orientation [59, 60], are feasible. The finer details can be approximated either by an updated version of Young's approach, combined with a generic diffraction smoothing at the Descartes angles [17], or applying the respective Möbius shift, previously retrieved from raytracing for realistic drop shapes, to Debye series intensity data for spherical drops [38, 39]. While the qualitative result for the primary rainbow remains basically the same as for symmetric spheroids, the general insensitivity of the secondary against changes in the drop shape is lost. Nonetheless the consequences are not too severe, as the Möbius shift is small for the above-horizon segment of the secondary for solar elevations in the relevant range of  $0^\circ \dots 40^\circ$ . For completeness, it should be added that a perturbation approach for the full Lorenz–Mie solution was published about 20 years ago, and would in principle allow one to treat the case of 'hamburger bun' drops effectively, but has seemingly not yet been applied to objects of the size of typical raindrops [61, 62].

### *3.2. Drop size distribution, optical thickness, and rain shower geometry*

In a typical rain shower we will find a broad variety of drop sizes, i.e. a polydisperse mixture. This is expressed in quantitative terms through a density function called 'drop size distribution' (DSD), describing the number of drops per unit volume of air and drop size interval. The DSD will vary spatially (in all three dimensions) within a rain shower and also change over time. It can be determined for fixed positions on the ground by disdrometer techniques [63]. The results can often, but not always, be fitted well by a gamma distribution with the parameters  $n_0$ ,  $\mu$  and  $\Lambda$  [56, 64]

$$n(a_0) = n_0 \cdot (2a_0)^\mu \cdot \exp(-\Lambda \cdot 2a_0). \quad (1)$$

Traditionally, the drop diameter instead of the radius is used for fitting such gamma distributions, which explains the appearance of  $2a_0$  in this formula. Figure 5(c) displays several examples of DSDs measured during a receding shower (rainfall intensity varying from 0.3–0.06 mm min<sup>-1</sup>) and fitted by (1). As in the case of rainbows no absolute intensity measurements are of interest, the DSDs are relevant only in relative terms, i.e. the parameter  $n_0$  is not important here.

Rainbows caused by such polydisperse drop mixtures can, in principle, be modeled in a straightforward way by superimposing the scattering patterns of all individual drop sizes, taking into account the directly size-related effects such as color purity, supernumerary spacing, and total cross-section (see section 2) as well as influences from the non-spherical, size-dependant drop shape (see section 3.1). A broad DSD will typically diminish the number of visible supernumerary arcs, or often even completely extinguish their sequence. Matters are complicated by the fact that natural rainbows are ‘nonlocal’: all drops along the sunlit part of a generatrix of the rainbow cone can contribute to the specific ‘rainbow spot’ in this viewing direction (see figure 5(d)). Thus the appearance of the rainbow will not be determined by the DSD at a specific location alone, but by the integrated DSD along the effective line of sunlit drops (this will be further referred to as ‘eDSD’, standing for ‘effective DSD’, throughout this paper), assuming for the moment a sufficiently low optical thickness of the shower. Depending on the viewing direction, this can also include positions up to several 100 m above the ground, for which no reliable local DSD information can be obtained with ground-based disdrometers. If, as a first approximation, the DSD is assumed to be homogeneous throughout the whole rain shower, we will expect the brightest spots along the rainbow’s circumference at the positions corresponding to the longest line of sunlit drops. For low sun elevations and not too dense showers, these are typically the bases of the rainbow close to the horizon, which provides another reason why these parts appear often very intense [65].

These geometrical factors were, amongst others, addressed in detail by Gedzelman within a general model describing rainbows in their atmospheric environment to account for variations in brightness and colorization [35, 65]. In this model, a simple cuboid cloud and shower shape was assumed as a starting point (see figure 5(d)). Apart from effects such as the spectral composition of the incident sunlight, and further spectral deteriorations in the rainbow light due to scattering by air molecules and aerosols, the influence of the optical thickness of the rain shower volume is discussed as well. In dense rain showers the contribution of remoter raindrops can be diminished due to a pronounced self-extinction in the shower, i.e. further scattering of the rainbow light by other drops that lie in the way to the observer. In the extreme case, only the nearest layer of drops may generate a discernible rainbow, while multiple scattering in the remaining part of the shower will result in a gray background. This means that for showers with a considerable optical thickness, the contributing DSDs along the drop line have to be properly weighted to allow for a realistic rainbow modeling. Moreover, the diffuse background has to be added to the result.

In reality, the complex cloud shapes and resulting shadows being cast on the rainbow cone, together with spatially variable DSDs and optical thicknesses, make the full theoretical reconstruction of a real rainbow illumination and scattering situation almost impossible. Nonetheless, first attempts have been made to deduce the shape of the eDSD from calibrated rainbow photographs under simplified assumptions such as piecewise homogeneous local DSDs and low optical thickness [38] (see figure 8 in section 5). This illustrates that, in principle, rainbows can be used as remote sensing tools to determine physical properties of their generating rain showers. However, the analysis represents a typical ‘inverse problem’ as

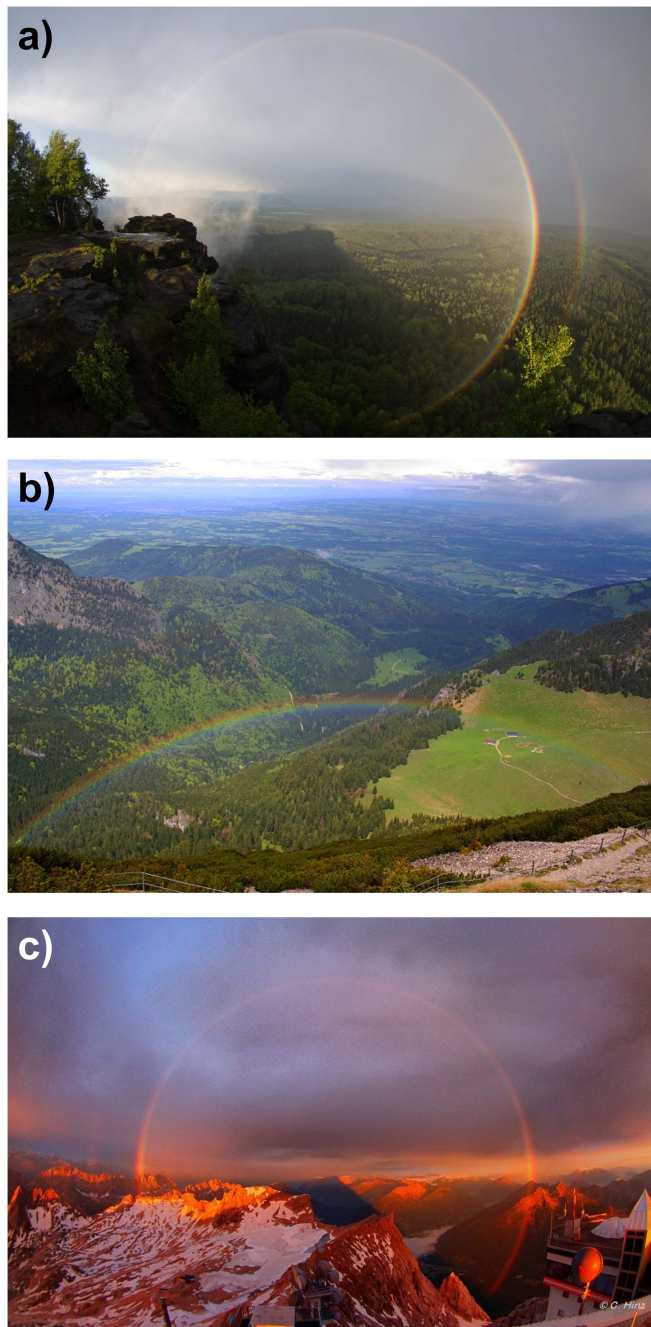


**Figure 6.** (a) Primary and secondary rainbow spanning about 3/4 of their full circumference above and below the horizon, photographed from a steep cliff (15 May 2016, Mt. Zschirnstein, Germany). (b) Bright primary and weak secondary rainbow at a high solar elevation of  $63.2^\circ$  (30 May 2010, Mt. Wendelstein, Germany). (c) Red rainbow above and below the horizon at sunrise (8 July 2014, Mt. Zugspitze, Germany). Photographs (b) and (c) taken by and reproduced with permission from C Hinz.

often encountered in scattering physics, and not much is known yet about the uniqueness and stability of the ensuing solutions for actual rain showers. For cloud droplets and the resulting cloudbows, such an approach has already been studied in more detail [66].

Finally, it should be noted that all these considerations are applicable only to rainbows which are due to genuine rain showers. ‘Rain’ bows can however be created by other drop sources as well, such as dewdrops on grass, crops and spider webs (‘dewbows’ [2, 67]), or artificial fountains (see figure 7(c)) and spray bottles. Though the rainbow cone geometry for incident sunlight still applies in these cases, the DSDs may turn out rather different than in the shower regime due to the physically different ways of drop generation.

## 4. Rainbows observed from special observation locations

### 4.1. High altitudes

Observers located on mountains or travelling in airplanes, balloons or gondolas have the rare chance to study the sub-horizon parts of rainbows, as under these circumstances many sunlit raindrops can be present below the horizon before the line of sight hits the ground. Marvellous photographs showing natural full-circle or nearly-full-circle rainbows were thus obtained (figure 6(a)) [68, 69]. Alternatively, quadcopters can be used to record the evolution of rainbows from the ground to higher altitudes [70]. These special locations also allow rainbow observations for solar elevations which are way higher than the traditional maximum values of  $42^\circ$  for the primary and  $51^\circ$  for the secondary, when the tops of these bows meet the horizon, respectively. At present, the highest documented solar elevation for a rainbow observation lies at  $63.2^\circ$ – $63.6^\circ$  (figure 6(b)) [71]. However, it seems likely that rainbows have already been filmed at even higher solar elevations over Hawaii, though the footage has not been analysed in detail as of now [72].

Elevated viewpoints are also well suited for the study of more exotic rainbow phenomena. Sub-horizon parts of rare twinned rainbows (see section 5) have been already photographed from a gondola [73]. At other occasions, pronounced kinks in the primary rainbow at the distant horizon were noted [74], which are likely caused by the cutoff of a more remote rain shower being visible above but not below the horizon, i.e. a sudden change in the eDSD. Such data are of high interest for the validation of rainbow models including non-spherical drop shapes and polydisperse DSDs (see section 3), since the accessible parameter space for ground-based observers is regrettably limited, compared with the full range of solar elevations and the complete rainbow circumference that can be treated by theoretical models [39]. High-altitude observations are moreover less disturbed by undesired aerosol scattering. It might be for this reason that the first detection of a quinary rainbow was accomplished from a mountain-based observatory (see section 6). Also, very dramatically illuminated sceneries of so-called ‘red rainbows’ extending far below the horizon at sunrise and sunset, i.e. caused by an effectively red light source, were documented from high altitudes (see figure 6(c)).

### 4.2. Near water surfaces

When rainbows rise above a calm water surface, it will be possible to observe their mirror images. However, the raindrops that contribute to the mirrored rainbows are located at a different position than those that make the direct bows [2, 4]. In this sense, rainbows have no ‘true’ mirror images, as e.g. local variations in the shower will have a slightly different impact

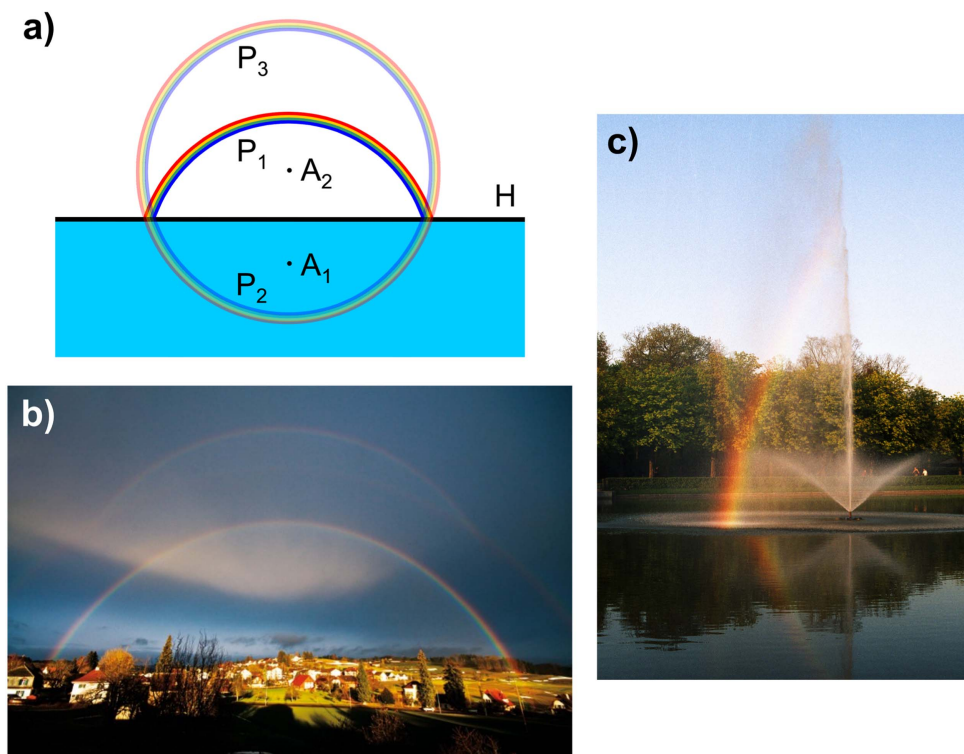


**Figure 7.** (a) Geometry sketch of the direct primary rainbow ( $P_1$ ), its mirror image ( $P_2$ ) and the reflected-light bow ( $P_3$ ).  $A_1$ : antisolal point (center of  $P_1$ ),  $A_2$ : antisolal point for the reflected Sun (center of  $P_2$  and  $P_3$ ), adapted from [2]. (b)  $P_3$  segment high on top of a direct double rainbow display including  $P_1$  and the secondary rainbow (skewed perspective due to the extreme wide-angle lens). Photograph taken by and reproduced with permission from M Frei. (c) Intersection of  $P_3$  and  $P_1$ , complemented by  $P_2$  appearing after a gap, seen at a park pond with a fountain. Note that due to this special source, water drops are also present below the horizon (marked by the intersection point), allowing  $P_1$  to extend some degrees further down.

on the direct and the mirrored bows. This difference is more pronounced the higher the observer is located above the water level.

More fascinating is a related effect that arises when the sunlight is allowed to be reflected on a water surface before it passes through the raindrops. In this case, the mirror image of the Sun acts as a second light source at a different—and in this case negative—elevation angle. Consequently, more than a half circle of such a ‘reflected-light rainbow’ can be seen above the horizon (see figure 7(a)). This large segment is complemented by the mirrored rainbow, resulting in the impression of a full circle around the reflected sun’s antisolal point  $A_2$  under perfect circumstances. Moreover, it may even happen that a ‘mirrored reflected-light rainbow’ becomes visible, which will then complement the direct rainbow to another full circle, in this case centered at the ordinary antisolal point  $A_1$  [75]. Low solar elevations are in any case favorable, as the intensity loss due to the reflection at the water surface is then less pronounced (a consequence of Fresnel’s formulas). Displays including bright reflected-light secondary bows are rare, but may gain considerable media interest when occurring [76]. Often, the mirroring surfaces are spatially restricted so that only parts of the reflected-light

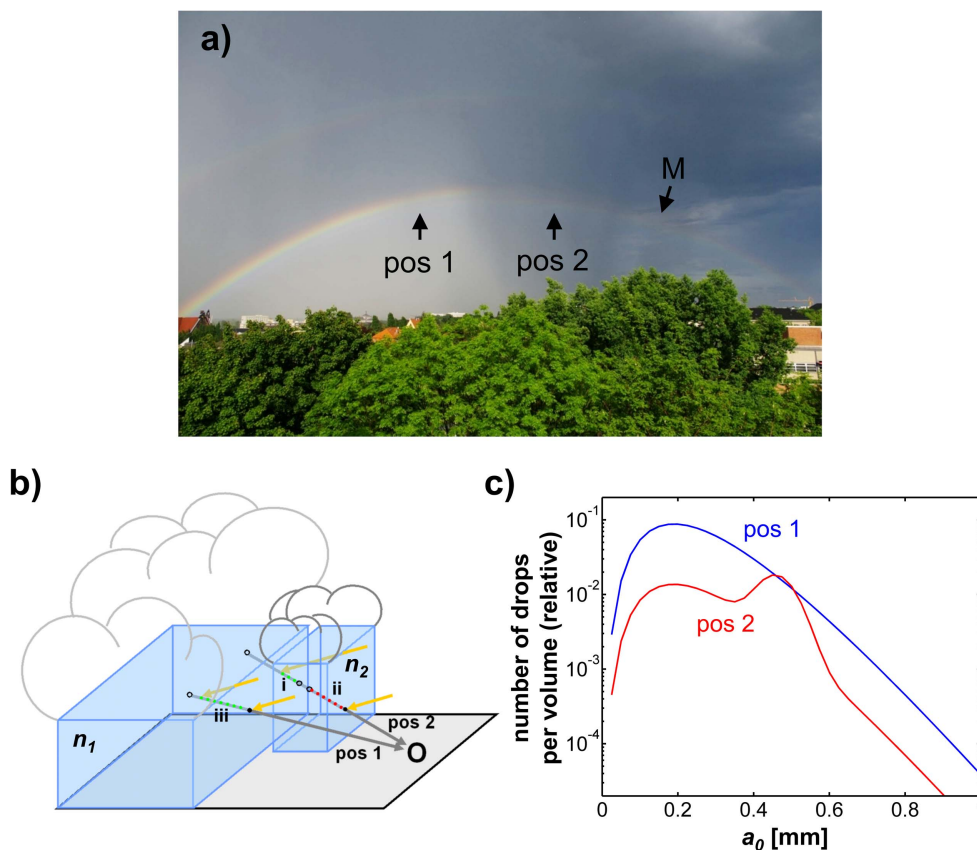


**Figure 8.** (a) Twinned rainbow observed on May 11th, 2012, Dresden. The twinning occurred only in the right half of the picture. M: approximate merging point of the two branches, pos 1/pos 2: selected positions for a reconstruction of the eDSD in the non-twinned and twinned part, respectively. (b) Simplified shower model for this observation. O: observer,  $n_1$ ,  $n_2$ : homogeneous local DSDs of showers 1 and 2, i and iii: effective segments of sunlit drops in shower 1, ii: effective line segment in shower 2. At pos 1, the observer sees only the rainbows generated by shower 1, at pos 2 a superposition of rainbows from showers 1 and 2 (reprinted from [38], with permission from OSA). (c) Reconstructed eDSDs for pos 1 (non-twinned) and pos 2 (twinned).

rainbows become visible. Two typical situations of reflected-light primary rainbows are depicted in figure 7(b) and (c): a mirror surface behind the observer will facilitate the visibility of the reflected-rainbow's top (b, for more details consult [77]). In contrast to this, for a mirror surface in front of the observer, i.e. towards the rainbow, the intersection of direct and reflected-light rainbows at the horizon will appear (c, for more details consult [78]). In rare cases, the reflected light bow has been observed even without the presence of a direct bow as a result of patchy rainfall or selective shadowing of the shower [79]. Reflected light rainbows will become blurred if the reflecting surface is corrugated due to the presence of small waves [80].

## 5. Twinned rainbows

Twinned rainbows are characterized by a branching of the primary rainbow into two arcs, one on top of the other, in the vicinity of its top. The color sequence, brightness and width of both these branches are comparable. Thus this phenomenon can clearly be distinguished from the more common sight of a primary accompanied by a supernumerary arc. Also the branches' separation is too small to allow for an explanation as an ensemble of direct and reflected-light rainbows (see section 4.2). The two branches merge into a single primary rainbow at some point further down along the circumference, giving the impression of an ordinary primary when meeting the horizon. Occasionally, only a part of the whole primary appears twinned (see figure 8(a)). Remarkably, the secondary bow usually shows no signs of twinning along the full visible part of its circumference [38, 81, 82]. A few anecdotal reports of related rainbow anomalies from the 19th and 20th centuries do exist; however, their identification as twinned rainbows is not fully reliable. The earliest unequivocal observation record dates back to 6 June 1979 at Reading, England [83]. Being a comparatively rare and short-lived phenomenon (with a typical duration of only some minutes), twinned rainbows have not yet become a subject of comprehensive statistical analyses. From the reports collected by the AKM e.V. [10] it can be estimated that they may occur about 1–3 times per year in Central Europe (combining the efforts of  $\sim 30$  observers<sup>2</sup>), but seem to appear more frequently in the English Midlands. A considerable number of accidental snapshots posted on internet image hosting platforms under the label of 'triple rainbows' demonstrates the world-wide occurrence of twinned rainbows.

Early explanations proposed that a mixture of liquid water drops and solid ice spheres would generate neighboring concentric rain- and icebows due to their slightly different indices of refraction. However, the observed branching effect and the lack of influence on the secondary bow could not be explained in such a way. A more promising step in another direction was taken at the suggestion of C Hinz at the 8th Light and Color Meeting in Bad Honnef, Germany, June 2004: a mixture of smaller and larger liquid drops in a rain shower may produce twinned bows due to the more pronounced shape distortion of the latter. These two sets of drops will generate two partially non-overlapping rainbows [84]. Raytracing simulations by L Cowley done during the same meeting backed up this hypothesis by reproducing the branching effect and also a non-twinned secondary bow [81]. Thus, the explanation of the twinned rainbow phenomenon was reduced to the question which kind of 'exotic' eDSD is needed to make them appear, provided that the rainbow theorists are in the possession of accurate models for the shape of natural raindrops and the ensuing rainbows. Remarkably, Venturi had already pointed out the same idea of two mixed drop sets with different shapes 200 years ago when setting up a short-lived non-interference theory for supernumerary arcs and the change in their appearance around the rainbow's circumference [36, 37]. Thus he was, accidentally, the first person to give the modern explanation for twinned rainbows, a phenomenon of whose existence he was very likely not even aware.

As described in section 3.1, the development of such models evolved over various approximate stages until a satisfactory level has now been reached. Concerning twinned rainbows, the next step in simulations beyond pure raytracing was the application of the Airy theory and classical Möbius shifts for symmetric spheroid drop shapes [85]. Later on, natural drop shapes and a more accurate optical model based on a refined Young raytracing approach were applied; however, these simulations used only a superposition of two distinct drop sizes

<sup>2</sup> Statistical data on atmospheric phenomena are collected from a stable group of 7–8 regular observers, but occasional highlights are also contributed by other people to the AKM's forum.

instead of a realistic polydisperse DSD [17]. Recently, the inclusion of multiple drop sizes into a model of Debye series intensity data shifted by the appropriate amounts for natural drop shapes finally allowed one to reconstruct the eDSD for a twinned rainbow from a calibrated photograph (see figures 8(b) and (c)) [38].

A surprising consequence from these polydisperse simulations is that, when starting with a model DSD from scratch, a pronounced twinning can be obtained by choosing a simple exponential distribution (described by formula (1) for  $\mu = 0$ ) with a typical value of  $\Lambda = 4 \text{ mm}^{-1}$  (as noted,  $n_0$  is not relevant for normalized rainbow intensities), and adding a single Gaussian peak centered around  $a_0 = 0.5 \text{ mm}$  [39]. The additional (and already considerably distorted) drops from the Gaussian peak are responsible for the lower branch, while the upper one is created by the underlying broad exponential DSD itself, in which nearly spherical drops around  $a_0 = 0.3 \text{ mm}$  (see figure 5(b)) provide the dominant intensity contribution. This is due to the fact that the intensity contribution from each drop size is not only determined by the number of these drops alone, but has to be multiplied with the size-dependent scattering cross section (varying with  $a_0^{7/3}$  in the Airy theory [7]).

Due to the non-local nature of the eDSD as a quantity integrated along the line of sight (see section 3.2), it is impossible to decide without further information whether a certain twinned rainbow is caused by two successive showers with different local DSDs or by a single shower with a non-typical, but otherwise rather homogeneous local DSD (i.e. exhibiting a secondary peak). From the author's experience, both situations do occur in nature. Some hints about the drops' distances can be obtained by analyzing the glittering of raindrops while rainfall still persists close to the observer. Each nearby drop will create a bright rainbow streak as it crosses the rainbow cone during its fall, when being photographed with a proper exposure time. If some of the recorded streaks coincide with the upper branch of the twinned bow, and others simultaneously with the lower, one may conclude that a homogeneous drop mixture is present [86]. On the other hand, it may happen that all recorded streaks belong only to one branch, which then indicates that the different drop sizes are separated in space and seen one after another (see figure 8(b), pos 2) [38]. Moreover, any kind of additional data such as simultaneous observations from other locations or ground-based precipitation gauge readouts may help to de-entangle the information condensed in the eDSD.

The reported stability of the secondary rainbow against twinning is due to the fact that the corresponding Möbius shifts are rather small in the solar elevation interval at which rainbows are commonly observed ( $0^\circ \dots 40^\circ$ ) (see section 3.1). This means that each drop size will yield a secondary rainbow which approximately overlaps with the ones stemming from the other sizes, and this coincidence property is independent of the eDSD. Moreover, as the angular width of the secondary is larger (see table 1), a larger shift would be required anyway to create a discernible twinning. Simulations indicate that a twinning at the top of the secondary may occur for solar elevations higher than  $50^\circ$ , i.e. just when the top meets the horizon or has already dipped below it. As rainbow observations under these circumstances are still possible from high altitudes or by using quadcopters (see section 4.1), it might only be a matter of time until the first genuine photograph of a twinned secondary will be published. Moreover, simulations indicate that also the tertiary and quinary rainbows, which have already been photographically detected in nature several times (see section 6), might show twinning effects [39].

If, as seen, a primary rainbow can split into two branches, a very natural question would be if splittings into three (or even more) of them may also occur in nature. Indeed, two cases of such a rare triple splitting have already been documented (Y-S Chang and T-C Chang, 24 July 2012, Yilan, Taiwan [87]; K Tashima, 5 August 2012, Yobuko, Kyushu Island, Japan [88]). Regrettably, the orientation data of the photos could not be determined with the

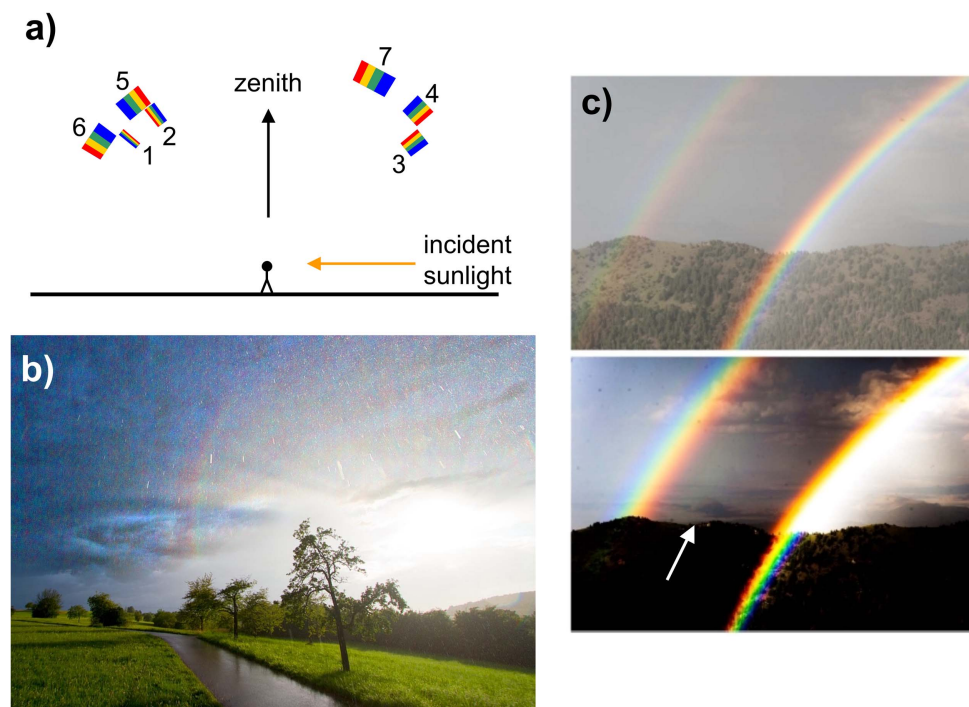


**Figure 9.** (a) Sketch of the celestial positions of the first seven rainbow orders for a sun at the horizon (elevation angle  $0^\circ$ ) (adapted from [6]). (b) Tertiary and quaternary rainbows, 4 August 2014, Kämpfelbach, Germany. Local contrast enhancement (unsharp masking) had to be applied to make the bows visible. Photograph taken by and reproduced with permission from M Großmann. (c) Quinary rainbow embedded in Alexander's dark band. Upper image: original, lower image: contrast enhanced version. The broad green/blue band of the quinary is marked by the arrow. Photograph taken by H Edens and reprinted from [96], with permission from OSA.

accuracy needed to perform a reliable DSD reconstruction (see section 8). Finally, it should also be mentioned that observations of twinned rainbows exist, which cannot be explained within the current theory of flattened drops, e.g. the display photographed by M Worme on 18 November 2009 in Barbados [89]. In this case, a branch of the primary rainbow extended into Alexander's dark band, though the Möbius shifts for the top of the primary can only account for a displacement away from Alexander's band, i.e. towards the antisolar point. Speculations about the cause of this phenomenon range from non-vertical drop axes, non-equilibrium (i.e. elongated instead of flattened) drop shapes, to impurities in the water resulting in a changed refractive index. While transient elongated states during drop oscillations can be ruled out due to the high oscillation frequencies ( $>100$  Hz [55]), which will wipe out any stable visual impression, axes canting might be caused by shear winds, and stable elongated drop shapes might result from strong vertical electric fields under cumulonimbus clouds [47].

## 6. Higher-order rainbows

Centuries ago, the duplicity of our familiar primary and secondary rainbows has already raised the question if even more than these two bows can appear under special circumstances. Newton erroneously believed that the directly transmitted rays (without any internal reflection, class 0b in figure 2(a)) might give rise to a ‘zero-order’ rainbow. As we know today, no such zero-order bow exists, since the deflection function for these rays, as well as for class 0a, does not exhibit any extremum [90]. On the other hand, all rays of classes 3 and higher do possess this property, thus we would expect the corresponding higher-order rainbows to occur in nature. Remarkably, the tertiary and quaternary rainbows should appear in the sunward direction of the sky at scattering angles of about  $40^\circ$ – $50^\circ$ , while the quinary rainbow would be located within Alexander’s dark band (see table 1 and figures 2(c) and 9(a)).

Naturally, interest focused mainly on the tertiary rainbow (i.e. the first ‘unusual’ rainbow), whose angular position was first calculated by Newton and Halley. However, many of the historical observation reports of ‘tertiary rainbows’ do in fact describe other optical phenomena such as supernumerary rainbows, reflected-light rainbows, or ice-crystal halos. Dismissing these, only a handful trustable observations remain over the course of the past 250 years until 2011 [91].

There are several reasons which render the tertiary (and the other higher-order rainbows) almost invisible: firstly, each internal reflection very likely leads to a decrease of intensity, as these reflections are never total for nearly spherical drops, and shape distortions (see section 3.1) have to become rather pronounced to facilitate total internal reflections. Secondly, the angular dispersion increases with the rainbow order, i.e. the width of the colored bow becomes larger (see table 1 and figure 9(a)), thus leading to a further intensity reduction. Finally, the most important obstacle hindering observations of the tertiary and quaternary rainbows is that they have to compete against the bright zero order glow on the sunward side of the sky, which drastically reduces their contrast (see figure 2(c)). Note that this background is intrinsic, i.e. created by the very same drops as the rainbows, and will thus be present even under the best observing conditions. Moreover, the extrinsic background from skylight, clouds or multiple scattering will further impair the visibility in nature. Calculations indicate that the tertiary rainbow will just exceed the threshold of human perceptibility, especially when the natural oblateness of the raindrops is taken into account [39, 45, 91]. As it is, like all rainbows, strongly azimuthally polarized, its visibility can be enhanced by a linear polarizer which partially suppresses the weakly radially polarized zero-order glow [11].

In single-drop laboratory experiments, the detection of tertiary and other higher-order rainbows has already been accomplished a long time ago [92, 93]. However, it was only in 2011 that the first genuine photographs of natural tertiary rainbows were obtained (M Großmann, 15 May 2011, near Karlsruhe, Germany [94]; M Theusner, 11 June 2011, near Bremerhaven, Germany [95]), after the interest in chasing higher-order rainbows had been revived by the presentations of P Laven and R L Lee at the 10th Light and Color meeting in Maryland, USA, in 2010. Strong contrast enhancement had to be applied to the raw photos to extract recognizable traces of the rainbows (see figure 9(b)); nonetheless they are unequivocally recorded, as shown by additional quantitative analyses of the photographic data. Großmann also reports a very weak, shimmering visual impression. Theusner’s pictures represent furthermore the first photographic documentation of the quaternary rainbow, which lies right outside the tertiary. Meanwhile, about 35–40 photographic documentations of tertiary or both tertiary/quaternary bows from various observers and observing places have been published or communicated to Großmann (who decided to collect these data), but capturing them is still far from being a routine matter even for skillful rainbow observers. So far, no

claims of a successful visual observation of the quaternary do exist, though the chances are only slightly less as compared to the tertiary [11].

Concerning the quinary rainbow, it was expected that its first capture in a photograph might even precede the tertiary and quaternary bows, as its broad blue and green parts have only to stand out against the much lower intrinsic background in Alexander's dark band (its red rim will unfortunately be lost in the red of the much brighter secondary rainbow, see table 1 and figure 9(a)). Nonetheless, the first successful photographs, taken by H Edens, were published later [96]. In his publication he presents a detailed analysis of an observation from 8 August 2012 (Langmuir Laboratory for Atmospheric Research, New Mexico, 3240 m altitude, see figure 9(c)) and a list of nine other photographs of quinary rainbows from New Mexico taken during 2009–2013. Again, visual detections have not been reported, but the possibility is not to be ruled out [11].

The reproduction of these photographic observations from other locations turned out to be surprisingly difficult, although many pictures of bright primary and secondary rainbows have been checked for suspicious green and blue features in Alexander's dark band. Very likely, high observation altitudes and clear air are very favourable conditions for successful observations. Furthermore, extracting weak quinary rainbow traces from photographs is not a trivial task due to the presence of the bright primary and secondary arcs, which are prone to cause artifacts in the processing, and also afterimages in the perception of the processing operator. Nonetheless, it seems that finally a few other cases could be pinned down recently after a careful analysis [97].

No photographic or visual reports are known for the senary rainbow, which is embedded in the bright inner disk of the primary rainbow (see figures 2(c) and 9(a)). This intrinsic background is also partially polarized in azimuthal direction (consequently, a polarizer will not help much to increase the visibility of the senary). The chances are better for the septenary, as the background is again slightly radially polarized. Edens captured a stack of photographs which might show traces of a septenary rainbow in a filtered version of the composite image (22 September 2013, New Mexico) [98]. More observations are needed for a definite assessment of this case. Chances for the detection of even higher rainbow orders in nature are considered low [11]. A synopsis of all reported photographic detections of tertiary, quaternary and quinary rainbows up to 31 December 2013 is also presented in [11].

## 7. Divergent-light rainbows

Up to now, it was assumed that only the Sun may serve as the rainbow-generating light source. It has been known for a long time that the Moon, when close to the full phase, can also produce rainbows [4]. These are fully equivalent to the familiar solar rainbows, the only difference is that they usually appear white to the human eye due to their low intensity.

We face a qualitatively different situation only when rainbows are created by nearby artificial light sources. For simplicity, the discussion will be restricted to an idealized point-like source emitting non-parallel light rays from its position ('divergent light'). In reality, a pocket lamp light bulb or LED without any collimating optics may come close to this ideal case, but street lamps can also be regarded this way if the observer is sufficiently far away (i.e. some meters). Street lamp induced dewbows have indeed been occasionally observed, exhibiting an unexpectedly complex shape compared to solar or lunar dewbows [99–102]. Similarly strange rainbows have been observed in lighthouse and searchlight beams poking through rain showers [103–105]. On the other hand, when a (nearly) isotropic light source is placed in a homogeneous rain shower, the observer will merely see the ordinary primary and

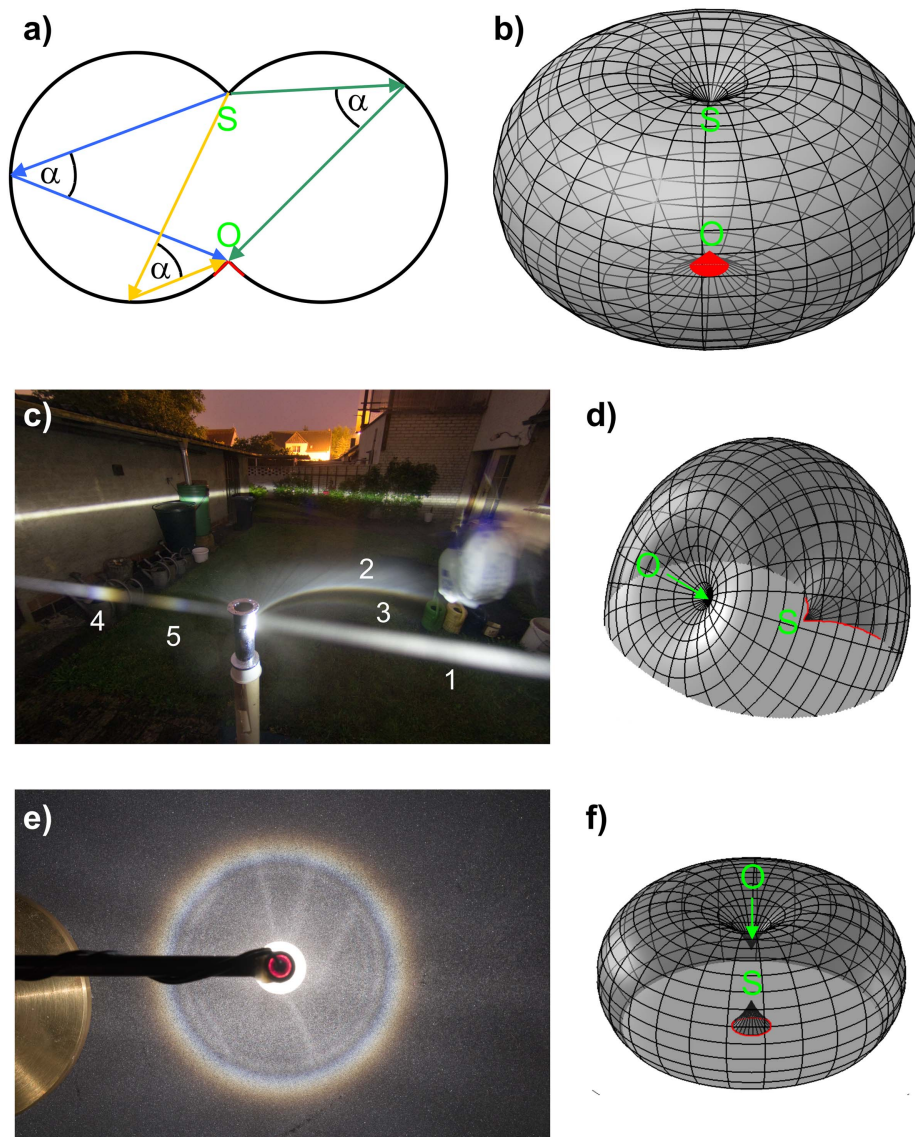


**Figure 10.** (a) Possible locations (black lines) for raindrops scattering light from the source  $S$  under the angle  $\vartheta = 180^\circ - \alpha$  to the observer  $O$  in a planar section through  $S$  and  $O$ . (b) Corresponding surface in 3D space (Minnaert apple). The parts marked in red in (a) and (b) are responsible for the generation of rainbows in nearly parallel light. (c) Lighthouse-type divergent-light rainbow in water drops from a spray bottle. 1: incident beam of light (coming in from the right), distributed into a disk of light by the cylindrical mirror, 2: primary rainbow branch, 3: secondary rainbow, 4, 5: primary and secondary rainbows due to the part of the incident beam that misses the mirror. (d) Corresponding Minnaert apple geometry for the primary rainbow, the red line marks the branch visible in (c). (e) Primary glass bead bow accompanied by supernumerary arcs in reverse geometry, i.e. behind the light source (radius of glass beads  $a_0 \approx 0.05$  mm), (f) Corresponding Minnaert apple geometry for the reverse glass bead bow.

secondary rainbows in the direction of the traditional rainbow cone, though somewhat more diffuse than in the case of solar illumination. How can this multitude of different effects be explained?

It turns out that the traditional rainbow cone geometry requires some modifications to deal with the case of divergent light. As seen from figure 10(a), all water drops that scatter light under the same angle  $\vartheta = 180^\circ - \alpha$  (with  $\alpha \approx 42^\circ$  for the primary rainbow) from the source S to the observer O have to be located on two circular arcs in any section plane through O and S. This is a direct consequence of the geometric theorem of equal peripheral angles. Due to rotational symmetry, all these drop positions allowing for successful scattering are located on an apple-shaped surface (figure 10(b)) in 3D, obtained by rotating the 8-like figure from figure 10(a) around the axis through S and O. From a mathematical viewpoint, this object can be regarded as a generalized torus, at which no central hole remains as the generating rotating circle intersects itself. For the case of ice crystal halos in the forward scattering regime ( $\vartheta \approx 22^\circ$  and  $\vartheta \approx 46^\circ$ ), this surface is usually called ‘Minnaert cigar’ [106, 107]—here, the name ‘Minnaert apple’ seems more appropriate.

Remarkably, on the primary rainbow’s Minnaert apple, the part close to the observer (marked in red in figures 10(a) and (b)) can be locally approximated well by a cone, which turns out to be nothing else than the traditional rainbow cone. This is immediately clear when we, for once, also regard the Sun as a point source in finite distance—the gigantic Minnaert apple in interplanetary space between Earth and the Sun only encounters water drops in the Earth’s atmosphere, i.e. very close to O (compared to the distance between O and S). Alternatively, one can say that the cone approximation is valid as long as the rays from the source can be regarded as nearly parallel in the vicinity of the observer.

When the full space between and around the observer and an artificial light source at some meters distance is occupied with water drops, one might expect the whole Minnaert apple to become visible. However, only rather diffuse rainbows at their traditional positions are then observed. This is due to the fact that when seen from point O (which is the only valid position to view into the Minnaert apple, as one cannot simply ‘step out’ and watch it under the outside perspective of figures 10(b), (d) or (f)), drops on the respective approximate cones (see figure 10(b)) will add up their rainbow intensities like in the solar case. For all other positions on the apple, such a nearly tangential view is not possible, hence the scattering intensity is drastically diminished. Moreover, all colors will be mixed up to white at these positions, as each color possesses a slightly different Minnaert apple shape and all these differently colored layers will send scattering light under the same viewing direction to the observer. Only around the traditional rainbow cones a pronounced color separation is allowed to occur. Finally, restrictions of the light source have to be taken into account, as often such experiments are carried out using car headlights which emit only into a limited solid angle [108].

Nonetheless, it is possible to study the peculiarities of the Minnaert apple apart from its cone-shaped end vertex. These two options are either to restrict the positions of the scatterers (dewbow geometry) or to confine the illumination to a plane (lighthouse geometry). In both cases, only the intersection curves of the confinement planes and the Minnaert apple become visible. Figure 10(c) depicts such a lighthouse scenario: a cylindrical mirror (a chromium-plated bedpost) creates a horizontal disk of light when illuminated with a collimated beam (1) from a high-power white LED (entering the photo from the right), while water drops were provided by a spray bottle. The primary rainbow’s branch (2) is clearly visible on the right hand side of the mirror, according to the geometry presented in figure 10(d). Furthermore, the branch of the secondary rainbow (3) is faintly visible, as well as rainbow spots (4, 5) resulting from the remaining part of the incident beam. Alternatively, a laser beam reflected from a

rotating plane mirror can be used as a light source for such experiments [109]. Note that in all these lighthouse geometries, the section plane necessarily has to contain the source S.

A broader range of rainbow shapes can be accessed in the dewbow geometry, as both the source S and observer O can be placed arbitrarily above the ground plane containing the scatterers. The variety of possible geometries of different intersections or tangential contacts between the plane and the Minnaert apple allows colored bands and loops of varying thickness to appear. As favorable observing conditions do not occur too often in nature, it is more convenient to carry out tabletop experiments using spherical glass beads (intended to be used for surface grinding, suitable diameters range from 0.1 mm to 0.5 mm) spread on a black plate. Under these conditions, it is now possible to study e.g. the symmetric case of circular glass bead bows which appear behind the light source rather than behind the observer (figure 10(e)) ('reverse rainbows'). In the geometry sketch figure 10(f), the different Descartes angle for glass ( $\vartheta \approx 158.5^\circ$ ,  $\alpha \approx 21.5^\circ$ ) due to the higher index of refraction has been taken into account, resulting in a slightly different shape of the Minnaert apple. The angular size of such reverse rainbows is not fixed, but varies strongly with the height of the light source above the bead plate. Also the second, larger intersection circle and the merging of both can be easily made visible [110].

Finally, as it was mentioned that ordinary solar rainbows represent a limiting case for water drops which are restricted to the immediate vicinity of the observer O, one might ask what happens if the drops are allowed to exclusively occupy positions very close to the source S only. From the previous reasoning it is clear that under these conditions, reverse rainbows can exhibit arbitrarily small angular sizes. It has in fact been suggested to try to detect the presence of water in the atmosphere of exoplanets by analyzing polarization features from rainbow scattering. These would periodically occur as the planet passes through the intersection points of its orbit and the Minnaert apple. Nonetheless, the angular radius of such extreme reverse rainbows, i.e. the angular distance between star and planet, will be practically zero [111].

## 8. Hints for photographing rainbows in nature

Taking photographs of 'ordinary' primary and secondary rainbows comparatively simple, and any camera can be used to photograph rainbows visible to the naked eye. However, to compress the whole width of both these rainbows on a single frame, one needs a fisheye or super wide angle lens, which basically restricts the choice of cameras to systems with interchangeable lenses. Due to the color dispersion, certain parts of the rainbow band easily get overexposed in one color channel, though the color saturation is not as complete as one might expect [6, 26]. In this respect, a slight correction of the automatically generated exposure value towards shorter times is helpful. If in doubt, or when taking pictures of rapidly changing phenomena, an automatically generated exposure bracket of 2–3 different settings may be applied.

A few more issues have to be taken into account when one aims at chasing the more rare phenomena such as twinned or higher-order bows. A large field of unobstructed view is desirable, which means that the observations should be either carried out in open rural areas or from the higher windows of large buildings. However, traditional windows allow only the view of one half of the sky, thus one will have to decide between a good view on the primary and secondary rainbows (also including the quinary rainbow, or twinning effects of the primary), or a promising viewpoint for the detection of the tertiary and quaternary bows. At best, one gets access to the roof or the skylight windows embedded therein. When doing so,

there is however the risk that raindrops accumulate at the front lens and spoil the photograph, or even create artifacts such as ‘false rainbows’ or anomalous blurred parts along the rainbow [112]. Some kind of protection such as an umbrella or cardboard shield can help to prevent this problem.

Photographs which are intended to serve as basis for a detailed analysis should always be recorded in the camera raw format in order to circumvent artifacts from compression or internal processing. Keeping track on synchronizing the camera clock can be a tiresome task, therefore it is more advisable to take a photo of a radio-controlled watch’s display shortly after the rainbow observation. Comparing the photographed display and the actual timestamp of the image file allows to reconstruct the camera clock offset and thus to precisely determine the points in time at which the rainbow photographs were taken.

Moreover, detailed analyses such as a eDSD reconstructions require a calibration of the photograph. This includes to determine (1) how angular distances between terrestrial or celestial objects are mapped onto the sensor (the ideal formulas for rectilinear and fisheye projections are known, but real lenses tend to differ more or less from that), and (2) how the camera is oriented spatially (i.e. into which directions in azimuth and elevation the optical axis is pointing, and about which angle the lower base of the sensor is rotated around this axis). This calibration task can be solved in a simple way by taking additional starfield photos, as the angular positions of stars (or planets) can be calculated with great precision. For task (1) it is straightforward to measure the distance of  $\sim 20$  stars from the sensor center in pixels on a starfield photograph, plot them versus their respective angles to the optical axis, and finally fit a suitable function to this dataset. Of course both the rainbow and the starfield picture have to be photographed with the same lens at the same focal length. As it is difficult to precisely reproduce a certain focal length within the variable range of a zoom objective, choosing an edge value (e.g. the shortest focal length) is recommendable.

Task (2) is a bit more complicated, as the three angles cannot usually be measured accurately enough when taking the photograph. It is, however, possible to calculate them from (at least) two reference objects in the picture, for which the coordinates in azimuth and elevation must be known. However, such data are again not available under normal circumstances, or very likely not precisely enough. The easiest solution, which requires no additional measurement devices, is to take another starfield image from the very same spot from which the rainbow observation was made. This image has to include both the chosen reference objects, though it is not necessary to precisely reproduce the orientation angles of the previous rainbow photograph. Now the starfield picture itself can be calibrated by two stars (with known coordinates) serving as references, and from that the coordinates of the terrestrial reference objects can be calculated. This information allows to determine the orientation angles of the initial rainbow picture. This procedure has been carried out successfully several times by the author [38, 94] and can be as accurate as  $0.1^\circ$  throughout the whole image. Of course, a crucial requirement is that the calibration starfield picture must indeed be taken as close as possible from the same spot as the rainbow image. Otherwise, the position coordinates of the references will suffer from parallax errors. For the same reason of error minimization, rather remote objects (distance  $> 100$  m) should be chosen as references. Finding the spot again with the necessary accuracy of  $\pm 20$  cm is easy for a window observation, but may be rather complicated in the outdoors. There, it is recommendable to somehow mark the feet or tripod positions on the ground for a return at night.

## 9. Summary and outlook

Rainbows are aesthetically pleasing phenomena that have rightfully become standard examples for the laws of optics on all levels of education in physics, though often being treated only cursorily. This, of course, is acceptable and even necessary for educational purposes, but it bears the risk that only very few people are actually aware of the marvellous complexity of natural rainbows in the end. Keeping a watchful eye (and camera lens) on the sky will, however, over time result in a collection of more or less uncommon observations that require further thinking beyond the usual textbook simplifications.

In this review, many observations and reasonings were presented that have their origin exactly in this watchfulness and curiosity. It has been illustrated that a realistic rainbow theory requires more than just the understanding of light scattering from a single and perfect water sphere in air, and that rainbows can be more than just two colored semicircles. This includes sub-horizon observations from mountains, reflected-light rainbows, the effect of twinning and the chase for higher orders. The familiar concept of parallel sunlight and the ensuing rainbow cone was extended to include the cases of divergent illumination from small light bulbs on a kitchen table as well as from remote stars. Finally, some helpful hints on how to photograph rainbows in a way that the resulting pictures can be used beyond the pure aesthetic impression for later scientific analyses were presented.

Of course, it is impossible to condense the whole ‘rainbow universe’ into one review. Topics not addressed here, but worth considering, include rainbows beyond the visible wavelength range, i.e. in the near infrared [4, 113] and ultraviolet [114]. Furthermore, polarimetric studies [115, 116] deserve attention, especially with regard to non-spherical drop shapes which may even result in weak circular polarization signatures [39]. Classroom or lab course projects might be inspired from various laboratory experiments complementing observations in nature [93, 117–122]. It should also be noted that rainbow scattering has already been technically applied for measurements of refractive index, temperature, and size of spray droplets [123, 124].

## Acknowledgements

All photographs, if not indicated otherwise, were taken by the author.

## References

- [1] Pernter J M and Exner F M 1922 *Meteorologische Optik* 2nd edn (Wien/Leipzig: W Braumüller Universitäts-Verlagsbuchhandlung) pp 527–602
- [2] Minnaert M 1954 *The Nature of Light and Colour in the Open Air* (New York: Dover) pp 167–90
- [3] Nussenzveig H M 1980 The theory of the rainbow *Atmospheric Phenomena, Readings from Scientific American* (San Francisco, CA: W H Freeman and Company) pp 60–71
- [4] Greenler R 1980 *Rainbows, Halos, and Glories* (Cambridge: Cambridge University Press) pp 1–21
- [5] Jackson J D 1999 From Alexander of Aphrodisias to Young and Airy *Phys. Rep.* **320** 27–36
- [6] Lee R L and Fraser A B 2001 *The Rainbow Bridge: Rainbows in Art, Myth, and Science* (University Park, PA: Pennsylvania State University Press)
- [7] Adam J A 2002 The mathematical physics of rainbows and glories *Phys. Rep.* **356** 229–365
- [8] Vollmer M 2006 *Lichtspiele in der Luft: Atmosphärische Optik für Einsteiger* (München: Spektrum Akademischer Verlag) pp 101–49
- [9] Arbeitskreis Meteore e.V. [www.meteoros.de](http://www.meteoros.de) (last accessed 24 July 2016)

- [10] Krämer P 2015 Die atmosphärischen Erscheinungen im Jahr 2014 *Meteoros* **18** 117–21  
 Krämer P 2014 Die atmosphärischen Erscheinungen im Jahr 2013 *Meteoros* **17** 60–3  
 Krämer P 2013 Die atmosphärischen Erscheinungen im Jahr 2012 *Meteoros* **16** 71–4 and previous years
- [11] Können G P 2015 Polarization and visibility of higher-order rainbows *Appl. Opt.* **54** B35–40
- [12] Laven P Mie plot <http://philiplaven.com/mieplot.htm> (last accessed 24 July 2016)
- [13] Fenn C *et al* Regenbogen in unserem Auge <http://forum.meteoros.de/viewtopic.php?f=2&t=5744> (last accessed 24 July 2016)
- [14] Cowley L The sky transform—why do we see patterns in the sky, rainbows, halos, glories..? <http://atoptics.co.uk/fz983.htm> (last accessed July 24 2016)
- [15] Hinz C Supernumeraries on primary and secondary rainbow <https://atoptics.wordpress.com/2013/07/20/supernumeraries-on-primary-and-secondary-rainbow/> (last accessed 24 July 2016)
- [16] Laven P Ray tracing with interference (Young’s method) <http://philiplaven.com/p8f.html> (last accessed 24 July 2016)
- [17] Sadeghi I, Munoz A, Laven P, Jarosz W, Seron F, Gutierrez D and Jensen H W 2012 Physically-based simulation of rainbows *ACM T. Graphic* **31** 1–12
- [18] Arago F 1828 Ueber ungewöhnliche Regenbögen *Ann. Phys., Lpz.* **91** 537–8
- [19] Airy G B 1838 On the intensity of light in the neighbourhood of a caustic *Trans. Camb. Phil. Soc.* **6** 379–403
- [20] Möbius W 1907 Zur Theorie des Regenbogens und ihrer experimentellen Prüfung *Abh. Kgl. Sächs. Ges. Wiss. Math.-Phys. Kl.* **30** 108–254  
 Möbius W 1910 *Ann. Phys.* **33** 1493–1558 (shortened version)
- [21] Können G P and de Boer J H 1979 Polarized rainbow *Appl. Opt.* **18** 1961–5
- [22] Lock J 2016 Limitations on the validity of light scattering models for high-order rainbows *Presentation at the 12th Int. Conf. on Light and Color in Nature (University of Granada, Granada, Spain)*
- [23] Lorenz L 1898 Sur la lumière réfléchiée et réfractée par une sphère transparente *Œuvres Scientifiques Tome Premier* (Copenhagen: Librairie Lehmann and Stage) pp 403–529
- [24] Mie G 1908 Beiträge zur Optik trüber Medien, speziell kolloidaler Metallösungen *Ann. Physik* **25** 377–445
- [25] Hergert W and Wriedt T 2012 *The Mie Theory: Basics and Applications* (Berlin: Springer)
- [26] Lee R L 1998 Mie theory, Airy theory, and the natural rainbow *Appl. Opt.* **37** 1506–19
- [27] Debye P 1908 Das elektromagnetische Feld um einen Zylinder und die Theorie des Regenbogens *Phys. Z.* **9** 775–8
- [28] van der Pol B and Bremmer H 1937 XIII. The diffraction of electromagnetic waves from an electrical point source round a finitely conducting sphere, with applications to radiotelegraphy and the theory of the rainbow—part I *Phil. Mag.* **24** 141–76  
 van der Pol B and Bremmer H 1937 LXXVI. The diffraction of electromagnetic waves from an electrical point source round a finitely conducting sphere, with applications to radiotelegraphy and the theory of the rainbow—part II *Phil. Mag.* **24** 825–64
- [29] Nussenzveig H M 1979 Complex angular momentum theory of the Rainbow and the glory *J. Opt. Soc. Am.* **69** 1068–79
- [30] Shen J and Wang H 2010 Calculation of Debye series expansion of light scattering *Appl. Opt.* **49** 2422–8
- [31] Beard K V and Chuang C 1987 A new model for the equilibrium shape of raindrops *J. Atmos. Sci.* **44** 1509–24
- [32] Chuang C C and Beard K V 1990 A numerical model for the equilibrium shape of electrified raindrops *J. Atmos. Sci.* **47** 1374–89
- [33] Thurai M, Huang G J, Bringi V N, Randeu L and Schönhuber M 2007 Drop shapes, model comparisons, and calculations of polarimetric radar parameters in rain *J. Atmos. Oceanic Technol.* **24** 1019–32
- [34] Thurai M, Szakáll M, Bringi V N, Beard K V, Mitra S K and Borrmann S 2009 Drop shapes and axis ratio distributions: comparison between 2D Video disdrometer and wind-tunnel measurements *J. Atmos. Oceanic Technol.* **26** 1427–32
- [35] Gedzelman S D 2008 Simulating rainbows in their atmospheric environment *Appl. Opt.* **47** H176–81

- [36] Venturi G B 1814 *Commentari sopra la storia e le teorie dell'ottica* (Bologna: Pe' Fratelli Masi e compagno) pp 166–80
- [37] Brandes H W 1816 Venturi's Theorie des farbigen Bogens, welcher sich oft an der innern Seite des Regenbogens zeigt, dargestellt mit einigen Anmerkungen *Ann. Phys. (Gilbert)* **52** 385–97
- [38] Haußmann A 2015 Observation, analysis, and reconstruction of a twinned rainbow *Appl. Opt.* **54** B117–27
- [39] Haußmann A 2016 Polarization-resolved simulations of multiple-order rainbows using realistic raindrop shapes *J. Quant. Spectrosc. Radiat. Transfer* **175** 76–89
- [40] Mishchenko M I, Travis L D and Mackowski D W 1996 T-matrix computations of light scattering by nonspherical particles: a review *J. Quant. Spectrosc. Radiat. Transfer* **55** 535–75
- [41] Fraser A B 1983 Why can the supernumerary bows be seen in a rain shower? *J. Opt. Soc. Am.* **73** 1626–8
- [42] Lock J A 1996 Ray scattering by an arbitrarily oriented spheroid. I. Diffraction and specular reflection *Appl. Opt.* **35** 500–14
- [43] Lock J A 1996 Ray scattering by an arbitrarily oriented spheroid. II. Transmission and cross-polarization effects *Appl. Opt.* **35** 515–31
- [44] Kokhanovsky A A and Nakajima T Y 1998 The dependence of phase functions of large transparent particles on their refractive index and shape *J. Phys. D: Appl. Phys.* **31** 1329–35
- [45] Langley D S and Marston P L 1998 Generalized tertiary rainbow of slightly oblate drops: observations with laser illumination *Appl. Opt.* **37** 1520–6
- [46] Können G P 1987 Appearance of supernumeraries of the secondary rainbow in rain showers *J. Opt. Soc. Am. A* **4** 810–6
- [47] Gedzelman S D 1988 Rainbows in strong vertical electric fields *J. Opt. Soc. Am. A* **5** 1717–21
- [48] Lock J A 2000 Supernumerary spacing of rainbows produced by an elliptical-cross-section cylinder. I. Theory *Appl. Opt.* **39** 5040–51
- [49] Adler C L, Phipps D, Saunders K W, Nash J K and Lock J A 2001 Supernumerary spacing of rainbows produced by an elliptical-cross-section cylinder. II. Experiment *Appl. Opt.* **40** 2535–45
- [50] Han Y P, Méès L, Ren K F, Gouesbet G, Wu S Z and Gréhan G 2002 Scattering of light by spheroids: the far field case *Opt. Commun.* **210** 1–9
- [51] Xu F, Lock J A and Tropea C 2010 Debye series for light scattering by a spheroid *J. Opt. Soc. Am. A* **27** 671–86
- [52] Lock J A and Xu F 2010 Optical caustics observed in light scattered by an oblate spheroid *Appl. Opt.* **49** 1288–304
- [53] Nye J F 1992 Rainbows from ellipsoidal water drops *Proc. R. Soc. Lond. A* **438** 397–417
- [54] Marston P L 1999 Catastrophe optics of spheroidal drops and generalized rainbows *J. Quant. Spectrosc. Radiat. Transfer* **63** 341–51
- [55] Szakáll M, Mitra S K, Diehl K and Borrmann S 2010 Shapes and oscillations of falling raindrops —a review *Atmos. Res.* **97** 416–25
- [56] Pruppacher H R and Klett J D 1997 *Microphysics of Clouds and Precipitation* 2nd edn (New York: Kluwer Academic Publishers) pp 30–8 and pp 400–8
- [57] Fraser A B 1972 Inhomogeneities in the color and intensity of the rainbow *J. Atmos. Sci.* **29** 211–2
- [58] Volz F E 1960 Some aspects of the optics of the rainbow and the physics of rain *Physics of Precipitation: Proceedings of the Cloud Physics Conference, Woods Hole, Massachusetts, June 3-5, 1959* ed H Weickmann (Washington, DC: American Geophysical Union) pp 280–6
- [59] Beard K V and Jameson A R 1983 Raindrop canting *J. Atmos. Sci.* **40** 448–54
- [60] Bringi V N, Thurai M and Brunkow D A 2008 Measurements and inferences of raindrop canting angles *Electron. Lett.* **44** 1425–6
- [61] Martin R J 1993 Mie scattering formulae for non-spherical particles *J. Mod. Opt.* **40** 2467–94
- [62] Martin R J 1995 Scattering matrices for slightly non-spherical particles *J. Mod. Opt.* **42** 157–69
- [63] Kathiravelu G, Lucke T and Nichols P 2016 Rain drop measurement techniques: a review *Water* **8** 29
- [64] Ulbrich C W 1983 Natural variations in the analytical form of the raindrop size distribution *J. Clim. Appl. Meteorol.* **22** 1764–75
- [65] Gedzelman S D 1982 Rainbow brightness *Appl. Opt.* **21** 3032–7
- [66] Alexandrov M D, Cairns B and Mishchenko M I 2012 Rainbow fourier transform *J. Quant. Spectrosc. Radiat. Transfer* **113** 2521–35

- [67] Arbeitskreis Meteore e.V. Taubogen <http://meteoros.de/bildergalerie/cat/92> (last accessed 24 July 2016)
- [68] Leonhardt C A full circle rainbow over Australia <http://starobserver.org/ap140930.html> (last accessed 24 July 2016)
- [69] Haußmann A Three quarters of a double rainbow 2016/05 <https://atoptics.wordpress.com//19/three-quarters-of-a-double-rainbow-plus-an-accidental-snapshot-of-a-tertiary-mt-zschirmstein-germany-may-15th-2016/> (last accessed 24 July 2016)
- [70] McKenna M Lissan house 360 degree full circle rainbow—Phantom 3 aerial footage <http://nightskyhunter.com/Lissan%20House%20Full%20Circle%20Rainbow%20-%20Drone%20Footage.html> (last accessed 24 July 2016)
- [71] Hinz C Arbeitskreis Meteore e.V. Regenbogeninvasion <http://forum.meteoros.de/viewtopic.php?f=2&t=7630&p=31439> (last accessed 24 July 2016)
- [72] Youtube user 'HK', Full circular double rainbow <https://youtube.com/watch?v=d0KJ5sFVUxw> (last accessed 24 July 2016)
- [73] Haußmann A Gondelfahrt in den Gespaltenen Regenbogen <http://forum.meteoros.de/viewtopic.php?f=2&t=55982> (last accessed 24 July 2016)
- [74] Edens H Discontinuous rainbow <https://atoptics.wordpress.com/2011/05/27/discontinuous-rainbow/> (last accessed 24 July 2016)
- [75] Cowley L Reflection rainbows <http://atoptics.co.uk/rainbows/reflect.htm> (last accessed 24 July 2016)
- [76] Lee J J Rarely observed 'quadruple' rainbow isn't what it seems <http://news.nationalgeographic.com/2015/04/150422-quadruple-double-rainbow-quaternary-tertiary-rain-atmosphere-science/> (last accessed 24 July 2016)
- [77] Frei M Double rainbow and reflected rainbow <https://atoptics.wordpress.com/2011/05/27/double-rainbow-and-reflected-rainbow/> (last accessed 24 July 2016)
- [78] Hinz C Reflected rainbow at a fountain <https://atoptics.wordpress.com/2011/05/14/reflected-rainbow-at-a-fountain/> (last accessed 24 July 2016)
- [79] Schmidt E and Hinz C Unpaired reflection rainbow <https://atoptics.wordpress.com/2016/06/27/unpaired-reflection-rainbow/> (last accessed 24 July 2016)
- [80] Cowley L Reflected bows and a not quite calm sea <http://atoptics.co.uk/rainbows/bowim47.htm> (last accessed 24 July 2016)
- [81] Cowley L Twinned rainbows <http://atoptics.co.uk/rainbows/twin1.htm> (last accessed 24 July 2016)
- [82] Arbeitskreis Meteore e.V., Gespaltener Regenbogen <http://meteoros.de/themen/atmos/wassertropfen/gespaltener-regenbogen/> (last accessed 24 July 2016)
- [83] Corliss W R 1984 *Rare Halos, Mirages, Anomalous Rainbows and Related Electromagnetic Phenomena* (Glen Arm, MD: Sourcebook Project) pp 7–10
- [84] Rendtel J and Hinz C 2004 Atmosphärische Optik am Rhein *Meteoros* **7** 91–5
- [85] Haußmann A 2008 Simulation des Gespaltenen Regenbogens mittels modifizierter Airy-Theorie *Meteoros* **11** 114–8
- [86] Haußmann A Rainbow twinning <http://atoptics.co.uk/fz1010.htm> (last accessed 24 July 2016)
- [87] Cowley L Anomalous bows <http://atoptics.co.uk/fz845.htm> (last accessed 24 July 2016)
- [88] Haußmann A Triple-split rainbow observed and photographed in Japan, August 2012 <https://atoptics.wordpress.com/2015/03/11/triple-split-rainbow-observed-and-photographed-in-japan-august-2012/> (last accessed 24 July 2016)
- [89] Hinz C Twinned rainbow <https://atoptics.wordpress.com/2011/05/27/twinned-rainbow-2/> (last accessed 24 July 2016)
- Cowley L Peculiar Rainbows <http://atoptics.co.uk/fz517.htm> (last accessed 24 July 2016)
- [90] Bohren C F and Fraser A B 1991 Newton's zero-order rainbow: unobservable or nonexistent? *Am. J. Phys.* **59** 325–6
- [91] Lee R L and Laven P 2011 Visibility of natural tertiary rainbows *Appl. Opt.* **50** F152–61
- [92] Billet F 1868 Mémoires sur les dix-neuf premiers arcs-en-ciel de l'eau *Annal. Sci. de l'Ecole Normale Supérieure* **5** 67–109
- [93] Walker J D 1976 Multiple rainbows from single drops of water and other liquids *Am. J. Phys.* **44** 421–32
- [94] Großmann M, Schmidt E and Haußmann A 2011 Photographic evidence for the third-order rainbow *Appl. Opt.* **50** F134–41

- [95] Theusner M 2011 Photographic observation of a natural fourth-order rainbow *Appl. Opt.* **50** F129–33
- [96] Edens H E 2015 Photographic observation of a natural fifth-order rainbow *Appl. Opt.* **54** B26–34
- [97] Haußmann A Three possible photographic detections of the natural fifth order rainbow from Germany <https://atoptics.wordpress.com/2016/08/16/three-possible-photographic-detections-of-the-natural-fifth-order-rainbow-from-germany/> (last accessed 16 August 2016)
- [98] Edens H E and Können G P 2015 Probable photographic detection of the natural seventh-order rainbow *Appl. Opt.* **54** B93–6
- [99] Mattsson J O, Nordbeck S and Rystedt B 1971 *Dewbows and Fogbows in Divergent Light (Lund Studies in Geography Series C No. 11)* (Lund: C W K Gleerup)
- [100] Mattsson J O 1998 Concerning haloes, rainbows and dewbows in divergent light *Weather* **53** 176–80
- [101] Gerber C 2005 Wandernde Bögen *Meteoros* **8** 108–9
- [102] Gerber C 2007 Erneute Beobachtungen des ‘reversen Lampenregenbogens’ *Meteoros* **10** 20–4
- [103] Floor C 1980 Rainbows and haloes in lighthouse beams *Weather* **35** 203–8
- [104] Harsch J and Walker J D 1975 Double rainbow and dark band in searchlight beam *Am. J. Phys.* **43** 453–5
- [105] Christoph A *et al* Seltsamer Bogen an einem Leuchtturm <http://forum.meteoros.de/viewtopic.php?f=2&t=5600> (last accessed 24 July 2016)
- [106] Tape W Streetlight halos <https://sites.google.com/a/alaska.edu/walt-tape/unpublished> (last accessed 24 July 2016)
- [107] Matsson J O, Barring L and Almqvist E 2000 Experimenting with Minnaert’s cigar *Appl. Opt.* **39** 3604–11
- [108] Fenn C 2006 Regenbögen im divergierenden Licht *Meteoros* **9** 58–62
- [109] Baader P and Arlt R 2008 Frühjahrstagung und Mitgliederversammlung des AKM 2008 *Meteoros* **11** 98–101
- [110] Haußmann A 2008 Beobachtung und Simulation des Glasperlenbogens in divergentem Licht *Meteoros* **11** 165–70
- [111] Bailey J 2007 Rainbows, polarization, and the search for habitable planets *Astrobiology* **7** 320–32
- [112] Großmann M 2013 The natural tertiary rainbow: a photographic first *Presentation at the 11th Int. Conf. on Light and Color in Nature (University of Alaska, Fairbanks, USA)*
- [113] Singhasaneh P Near Infrared rainbow <https://atoptics.wordpress.com/2011/06/22/near-infrared-rainbow/> (last accessed 24 July 2016)
- [114] Greenler R 2013 Recent rainbow revelations *Presentation at the 11th Int. Conf. on Light and Color in Nature (University of Alaska, Fairbanks, USA)*
- [115] Barta A, Horváth G, Bernáth B and Meyer-Rochow V B 2003 Imaging polarimetry of the rainbow *Appl. Opt.* **42** 399–405
- [116] Horváth G, Hegedüs R, Barta A, Farkas A and Åkesson S 2011 Imaging polarimetry of the fogbow: polarization characteristics of white rainbows measured in the high Arctic *Appl. Opt.* **50** F64–71
- [117] Sassen K 1979 Angular scattering and rainbow formation in pendant drops *J. Opt. Soc. Am.* **69** 1083–9
- [118] Simpson H J and Marston P L 1991 Scattering of white light from levitated oblate water drops near rainbows and other diffraction catastrophes *Appl. Opt.* **30** 3468–73
- [119] Großmann M ‘Spektrodrom’—a laboratory of rainbow <https://atoptics.wordpress.com/2013/11/30/spektrodrom-a-laboratory-of-rainbow/> (last accessed 24 July 2016)
- [120] Timusk T 2009 Flashes of light below the dripping faucet: an optical signal from capillary oscillations of water drops *Appl. Opt.* **48** 1212–7
- [121] Haußmann A Glass bead bow from a point-like light source <https://youtube.com/watch?v=sB0uLmFL8bc> (last accessed 24 July 2016)
- [122] Haußmann A Oil drop rainbow <https://youtube.com/watch?v=4Sx4cf1NmGA> (last accessed 24 July 2016)
- [123] Hattori H, Kakui H, Kurniawan H and Kagawa K 1998 Liquid refractometry by the rainbow method *Appl. Opt.* **37** 4123–9
- [124] Hom J and Chigier N 2002 Rainbow refractometry: simultaneous measurement of temperature, refractive index, and size of droplets *Appl. Opt.* **41** 1899–907